



Universidad Autónoma
de Madrid

Biblos-e Archivo
Repositorio Institucional UAM

Repositorio Institucional de la Universidad Autónoma de Madrid

<https://repositorio.uam.es>

Esta es la **versión de autor** del artículo publicado en:
This is an **author produced version** of a paper published in:

Applied Clay Science 124-125 (2016): 79-93

DOI: <https://doi.org/10.1016/j.clay.2016.01.043>

Copyright: © 2016 Elsevier B.V. This manuscript version is made available under the CC-BY-NC-ND 4.0 licence <http://creativecommons.org/licenses/by-nc-nd/4.0/>

El acceso a la versión del editor puede requerir la suscripción del recurso
Access to the published version may require subscription

Lime mortar-compacted bentonite-magnetite interfaces: an experimental study
focused on the understanding of the EBS long-term performance for high-level
nuclear waste isolation DGR concept.

Jaime Cuevas^{a*}, Ana Isabel Ruiz^a, Raúl Fernández^a, Elena Torres^b, Alicia Escribano^b,
Mercedes Regadío^a and María Jesús Turrero^b

^a Universidad Autónoma de Madrid. Facultad de Ciencias, Madrid, Spain

^b Centro de Investigaciones Energéticas, Medio Ambientales y Tecnológicas (Ciemat),
Madrid, Spain

*: corresponding author: jaime.cuevas@uam.es

Abstract

The aim of this study was to obtain evidences regarding the physical and geochemical processes occurring as a result of the combined effects of cementitious materials from the concrete degradation and magnetite from steel corrosion on the bentonite barrier during disposal of high-level radioactive waste.

A series of six experiments were done that attempt to reproduce the repository conditions prevailing from 1000 to 3000 years after emplacement of wastes. A lime mortar was used as the source of calcium and alkalinity as this is the presumed reactive product produced during concrete degradation at long-term. Magnetite powder was used to simulate the final corrosion product of cast iron and C-steel under anaerobic conditions. Either a natural FEBEX bentonite or a pretreated “aged” sample, depleted in exchangeable Mg and enriched in K, were used as the swelling clay component. Experiments, with both types of bentonite, were performed

1
2
3
4
5
6
7
8
9
10
11
12
13
14
15
24 simultaneously in cylindrical specimens (50 mm diameter, 25 mm length), confined in a
25 Teflon® sleeve/steel case cells. These specimens were composed of cement mortar in
26 contact with compacted bentonite, which was in turn in contact with compressed
27 magnetite powder. They were hydrated with an artificial Na^+ - Ca^{2+} - SO_4^{2-} -type Spanish
28 reference clayey formation water for 18 months at 60 °C and constant hydraulic
29 pressure applied through the base of the mortar..

16
17
18
19
20
21
22
23
24
25
26
27
28
29
30
31
32
33
34
35
36
37
38
39
40
41
42
43
44
45
46
47
48
49
50
51
52
53
54
55
56
57
58
59
60
61
62
63
64
65
30 After dismantling and sampling the specimens, distribution of soluble ions,
31 exchangeable cations and mineralogy were studied in the bentonite by different
32 instrumental techniques. Iron migration or any impact of the corrosion products in the
33 bentonite was not noticeable in the clay. Both, mortar and magnetite acted as sinks of
34 chloride and sulfate. Small quantities of Ca-Al-sulfates and carboaluminates, which can
35 allocate chlorides, were determined near the mortar-bentonite interface. Portlandite
36 dissolved near the bentonite interface and induced the formation of calcium silicates
37 hydrates (C-S-H) phases cementing the clay interface characterizing a calcium front
38 that was developed from the mortar towards the bentonite. Magnesium silicate
39 hydrates (M-S-H) phases were also concentrated at the interface with mortar in the
40 natural bentonite. It was also determined that natural bentonite has potentially higher
41 buffering capacity attenuating the calcium alkaline front than the pretreated clay. In
42 both cases, a low porosity bentonite-mortar zone was experimentally created at the
43 interface. This type of material should be carefully studied in order to predict the
44 potential for further development of a diffusive alkaline alteration, the radionuclides
45 retention and the consequences in the hydration rate of the unaffected bentonite
46 buffer.

Key words: Concrete, bentonite, alkaline alteration, lime mortar, long-term performance.

1 Introduction

The Deep Geological Repository (DGR) is currently the most accepted management option for the long-term isolation of high level radioactive wastes (e.g. U.S. DOE, 2014, NEA-OECD, 2003). Regardless of the geological options considered for the DGR, they all call for use of a multi-barrier system in order to achieve the safety requirements for limiting the eventual release of radionuclides to the biosphere.

The repository concepts associated with use of a clay host medium requires an engineered barrier system (EBS). For this case the EBS consists of a metallic canister surrounded by a bentonite buffer. For this geometry and geological environment there is also a requirement for the presence of a concrete annulus to provide mechanical support for the excavated galleries (e.g. in the Swiss concept: NAGRA, 2009). The use of concrete in the repository construction has the potential disadvantage of being the source of an alkaline front with the capacity to partially alter both the mineralogy of the bentonite (Gaucher and Blanc, 2006; Savage et al., 2007; Savage et al., 2010); or the mudstone host rock (Adler et al., 1999; Claret et al., 2002; Devol-Brown et al., 2007). Such a front also introduce calcium as the major cation available to exchange for other cations in the bentonite in the long term (Leguey et al., 2002; Techer et al., 2012). Many experiments have focused on the chemical behavior of clay when it is exposed to an alkaline plume at several temperatures. Most of them introduces Na, K-hyperalkaline fluids at pH >13, rather than lower pH environments dominated by

1
2
3
4
5
6
7
8
9
10
11
12
13
14
15
16
17
18
19
20
21
22
23
24
25
26
27
28
29
30
31
32
33
34
35
36
37
38
39
40
41
42
43
44
45
46
47
48
49
50
51
52
53
54
55
56
57
58
59
60
61
62
63
64
65

70 Ca(OH)_2 (pH 12.5) or C-S-H phases (pH < 12) as have been identified by Dauzères et al.,
71 2010. These authors outline the relative absence of representative experiments in real
72 clay/concrete interfaces, and their failure to take into account the effects of real
73 volumes and composition of solutions migrating through the porosities of the involved
74 materials. Moreover, even fewer papers have been dedicated to exploration of the
75 clay pore-water impacts on the concrete mineralogy and porosity.

76 It has been suggested that low-pH cements decrease the clay reactivity to insignificant
77 alteration (Berner et al., 2013, Bäckblom, 2005 and papers therein). In addition, these
78 studies show a good resistance of the system to saline (NaCl based) granitic ground
79 water aggression (García-Calvo et al., 2010). However, in these conditions an altered
80 front could be observed and characterized by the incorporation of magnesium ions
81 from ground water into the C-S-H gels (possibly forming M-S-H phases). In other
82 environments, when low-pH cement is compared to high pH CEM-I under the attack of
83 Na-Mg-Ca-sulfate, carbonated pore waters from Callovo-Oxfordian claystone pore-
84 waters (Dauzères et al., 2014; Gaucher et al., 2009), the low-pH cement matrix seems
85 easily damaged by chemical processes with the formation of a decalcification front and
86 the production of a silico-magnesian gel (M-S-H). The use of CEM-I was less reactive
87 because it is able to form a micrometric rim of calcite at the bentonite interface which
88 passivated further reactions. These observations state that the use of a low-pH cement
89 can release to the porewater significant concentrations of calcium. Similarly, the high
90 pH cements can release calcium in moderate carbonic environments. Dauzères et al.
91 (2014) and Jenni et al. (2014) have shown, in both, low-pH or high-pH concrete
92 interfaces, the role of carbonation and sulfate phases dynamics in producing porosity
93 changes in the concrete when they became in contact with clay pore waters or clay

1
2
3
4
5
6
7
8
9
10
11
12
13
14
15
16
17
18
19
20
21
22
23
24
25
26
27
28
29
30
31
32
33
34
35
36
37
38
39
40
41
42
43
44
45
46
47
48
49
50
51
52
53
54
55
56
57
58
59
60
61
62
63
64
65

94 materials. These materials can induce alteration process related to known reactions of
95 sulfate or magnesium attack environments (Menéndez et al., 2013; Santhanam, 2013).
96 The focus of this experimental study was to obtain evidences on the physical and
97 geochemical processes occurring by the combined effects of cementitious materials
98 generated from concrete degradation and from steel corrosion on the bentonite
99 barrier during storage and disposal of radioactive wastes. C-steel corrosion processes
100 will occur by a complex mechanism beginning with oxygen and/or water combined
101 with the effect of temperature. The release of Fe^{2+} by corrosion can result in several
102 corrosion products depending on the surrounding conditions. Experimental data from
103 Torres et al., 2007, indicate that there is a sequence of corrosion products, under
104 saturated and reducing conditions at the FEBEX bentonite/steel interface. Taking into
105 account the insignificant presence of carbonates in this bentonite, ferrous hydroxide is
106 the first reaction product, then magnetite is the most stable product, reached via
107 mixed Fe(II) and Fe(III) iron hydroxides, including green rust-Cl.
108 According to performance assessment simulations, after 1000 to 3000 years ,
109 anaerobic saturated conditions are expected to have developed near the canister
110 surface. Under these conditions the passivation of the steel surface will occur due to
111 the formation of a oxide, usually black in colour, protective film against further
112 corrosion. According to thermodynamics, magnetite will be the prevailing corrosion
113 product in environments without significant carbonate, silica or sulfide species activity
114 in solution because it is the end-member of the transformation of ferrous hydroxide
115 for cast iron and C-steel (Smart et al. 2002; King et al., 2014).

1
2
3
4
5
6
7
8
9
10
11
12
13
14
15
16
17
18
19
20
21
22
23
24
25
26
27
28
29
30
31
32
33
34
35
36
37
38
39
40
41
42
43
44
45
46
47
48
49
50
51
52
53
54
55
56
57
58
59
60
61
62
63
64
65

116 The design of the experiments described in this paper takes into account a situation
117 that represents a mid-long term stage in the repository as it is defined by several
118 generic argillite/shale disposal reference concepts (ENRESA, 2004, Yang et al., 2008,
119 Zheng 2014). This is to say conditions prevailing 1000 to 3000 years after emplacement
120 of the waste, when the bentonite is fully saturated. Montes et al. (2005) suggest in the
121 conclusions of their modelling work with the bentonite MX-80 that after 10000 years
122 of diffusion-reaction the barrier at the iron (canister-bentonite) interface could
123 virtually preserve with little changes the same physical–chemical (mineralogy) and
124 mechanical (swelling) properties. However, Samper et al. (2010), considering the
125 approach from Yang et al. (2008), calculated the concentration of interlayer exchanged
126 cations close to the bentonite FEBEX-concrete interface obtaining that after 1000 years
127 the bentonite is depleted in exchangeable magnesium. At this time, an active source
128 for calcium is still present at the concrete interface but without the hyperalkaline
129 conditions present earlier. On the other side, magnetite will be considered the stable
130 product at the surface of a steel canister. As a consequence, the experimental cells
131 used in this research are considered to be a small scale reproduction of the DGR
132 interfaces at mid-long term. Chemical fronts, mineralogical alteration and
133 microstructural effects are then studied under the scope of selecting relevant
134 phenomena for future description of reaction-transport processes and coupled
135 porosity evolution.

2 Materials and methods

2.1 EXPERIMENT CONCEPTUAL APPROACH

The design of the experiments was intended to reproduce the repository conditions prevailing 1000 to 3000 years after emplacement of wastes. This range of time was proposed based on the calculations reported in Samper et al. (2010). Furthermore, the experiments consider the interfaces present in the EBS, the concrete-bentonite interface at the hydration zone and the iron-bentonite interface on the opposite side (near the source of heat). Within this time period, the full hydration of bentonite, the homogenization of temperature at near 60 °C in the EBS, the depletion of Mg in the exchange complex of FEBEX bentonite (Ca, K-substituted in a 10 cm thickness at the concrete interface); and magnetite formation at the C-steel interface have been occurred. Most of these conditions, are predicted to prevail up to ten thousand years with the exception of the decrease of temperature to 40 °C (i.e. ENRESA, 2004).

2.2 MATERIALS

2.2.1 Natural and pretreated (aged) FEBEX Bentonite

The tests were performed with FEBEX bentonite, which has been selected by ENRESA (the Spanish Agency for Radioactive Waste Management) as a suitable material for the backfilling and sealing of HLW repository. The FEBEX bentonite was extracted from the Cortijo de Archidona quarry (Almería, Spain; Caballero et al., 2005). The physical-chemical properties of the FEBEX bentonite, as well as a summary of its most relevant thermo-hydro-mechanical and geochemical properties is shown in ENRESA (2006).

In order to reproduce a bentonite depleted in magnesium (FEBEX K, Na, Ca – from now referred to as **FEBEX pretreated**), natural FEBEX bentonite was soaked for 24 h in 1MKCl-1MNaCl-0.5M CaCl₂ aqueous solution. After this, the supernatant aqueous phase was discarded and this soaking cycle was repeated twice more using distilled water. The obtained slurry was allowed to air dry and then ground to pass a 1 mm sieve. **FEBEX natural** was also milled to 1 mm size for its use in the experiments. The **FEBEX pretreated** bentonite has a 13.0 ± 0.1 weight % water content under laboratory environmental conditions (30-40 % RH). The final distribution of exchangeable cations and the BET specific surface can be compared to FEBEX natural in Table I. This bentonite showed a decrease in cation exchange capacity (CEC), calculated as the sum of the charges of exchangeable cations. This reduction has led us to investigate, in terms of K-exchange, its impact on a presumably initial mineralogical transformation of the smectite component of bentonite.

Oriented aggregates were prepared by duplicate for a specific X-ray diffraction (XRD) study (Moore and Reynolds, 1997). Once the oriented films were air dried in the lab, one of the replicas was treated with ethylene-glycol vapor in order to expand the 001 montmorillonite lattice plane from its dry state (13 Å in the case of K-dominated form or 15 Å in the case of Ca-Mg form) to 17 Å (ethylene- glycol (EG) spacing for all cations-smectite species). The XRD patterns from natural or pretreated samples are shown in figure 1. Pretreated FEBEX was partially collapsed by the K-exchange treatment as indicated by the broader (001) and (002) d-spacings ($d_{001} = 16.2$ Å) and have non-regular angular positions. The modified 2:1 smectite structure behaves as a mixed layer mineral (MLM) including illite-like and smectite structures (40 % illite/60 % smectite type calculated using the Plancon and Drits (2000) software). In fact although

182 structurally similar to illite, they are not true illite. This is evidenced by the behaviour
183 during re-saturation of cation exchange positions with Mg and re-expansion in the
184 presence of EG vapor as they yielded a regular smectite (00l) d-spacing behavior, so
185 the effect is reversible. This behaviour would not be evident in a true illite. The same
186 effect was shown in previous studies in which montmorillonite was hydrothermally
187 treated (150-300 °C) in concentrated KCl or KOH solutions (Mosser-Ruck et al., 2001,
188 Mosser-Ruck and Cathelineau, 2004). Nevertheless, a significant decrease of CEC can
189 be explained by the collapsing effect of potassium, which is not completely reversible
190 to the cesium exchange practiced in the displacement method prepared to determine
191 the distribution of exchangeable cations.

2.2.2 Mortar, magnetite and Spanish reference argillaceous formation water composition

194 A lime mortar was prepared in order to provide a source for calcium and alkalinity
195 presumed to be an active process during concrete degradation. The lime mortar was
196 formulated as a 2:1 quartz-sand (< 0.5 mm particles diameter)/CaO (quicklime binder;
197 Stefanidou and Papayianni (2005)). CaO was obtained by heating Ca(OH)₂ Panreac™,
198 P.A. grade reagent at 950 °C for 1h, which was allowed to quench in absence of CO₂.
199 The mix was then combined inside a glove box by hand with a water/binder ratio = 1,
200 in a polypropylene cup. After the initial exothermic reaction for CaO hydration was
201 complete, the hydrated mix was pressed inside PVC mold rings of 50 mm diameter.
202 After hardening for 1 day it was allowed to cure for one month in a water vapor
203 saturated environment. The characteristics of this mortar, once saturated in water are
204 summarized in Table I.

Magnetite (Fe_3O_4) powder (1-5 μm) provided by Atlantic Equipment Engineers ref. (CAS-1317-61-9) was used for the experiments as received. The physical characteristics of the magnetite are: density: 4.8-5.1 g/cm^3 at 25 $^\circ\text{C}$ and molecular weight: 231.53 g. The water used to hydrate the cells is an artificial clay water ($\text{Na}^+ \text{-Ca}^{2+} \text{-SO}_4^{2-}$ type water) obtained in the laboratory after the analysis and synthesis of the water of a Spanish reference clayey formation. The solution composition includes the following concentrations: SO_4^{2-} 7.0×10^{-2} M, Cl^- 2.3×10^{-2} M, Na^+ 1.3×10^{-1} M, Mg^{2+} 8.2×10^{-3} M, $\text{Fe}^{(3+/2+)}$ 1.1×10^{-5} M, K^+ 8.2×10^{-4} M, Ca^{2+} 1.1×10^{-2} M, $\text{SiO}_{2(\text{aq})}$ 2.7×10^{-4} M and HCO_3^- 1.8×10^{-3} M at pH 7.5. (Turrero et al., 2001, 2006).

2.3 EXPERIMENTAL SETUP

A total of six experiments were performed simultaneously: two blank experiments with just bentonite (natural or pretreated); two double interface experiments with mortar-bentonite (natural or pretreated)-magnetite; and two single interface experiments with mortar-pretreated FEBEX bentonite or magnetite-pretreated FEBEX bentonite (Figure 2)

The tests were performed in a Teflon (glass fiber reinforced) cylindrical cells with an internal diameter of 5 cm and an inner length of 2.5 cm. The upper closing of the cells is made of a stainless steel plug, which allows to hydrate the composite material with water taken from a stainless steel pressurized reservoir (Figure 2). The bottom part of the cells is a plate of stainless steel.

Blocks of FEBEX bentonite were compacted with its hygroscopic water content (14-13%) at a nominal dry density of 1.65 g/cm^3 and placed inside each cell according to the scheme shown in Figure 2. In the cells 3 and 4 the magnetite powder was placed to provide a layer thickness of $\approx 2.0 \text{ mm}$. On top of this, the bentonite block ($\approx 18 \text{ mm}$) was inserted, then the mortar ($\approx 6 \text{ mm}$) and a stainless steel porous filter was installed above it. Hydration from the reservoir started as soon as setting-up of the cells finished and proceeded always through the upper part of the cell (with or without mortar) as it is vertically oriented in Figure 2. The deposit was initially pressurized with nitrogen at 5 bars. It was periodically detached from the cell and weighed, and this allowed checking water intake by the specimen. Experiments were run under isothermal conditions at 60°C inside an oven for 18 months. However, it was observed that there was no measurable water intake after approximately two months had passed.

2.4 Dismantling, Cutting and Sampling

The bentonite cylinders after dismantling had the appearance of a compact block including mortar interfaces. However, magnetite interfaces readily separated and part of it disaggregated in powder when the specimens were removed from the cells. Figure 3 shows the different subsamples cut from the specimens. Sample size was largely determined by the quantities needed to carry out the post-test analyses. The cutting machine (a diamond wire saw) had the cutting wire break during cutting of materials from cells 2, 3 and 4 (see numbers in Figure 2 and additional information file). When these breakages occurred, it was not possible to maintain the integrities of some of the longitudinal sections. In spite of this, longitudinal sections could be

manually re-assembled in order to study chemical fronts. The thicknesses uncertainties reported for the sampled slices are approximately within ± 1 mm.

2.5 Methods of analysis

2.5.1 Dry density, water content, soluble salts, exchangeable cations and adsorbed iron

The method used to determine the bulk density was the paraffin coating method (Blake and Hartge, 1986) applied to the small slices cut from the bentonite blocks extracted from the cells. Each of the subsamples shown in Figure 3 as DM, D and Fe were used to determine soluble elements in aqueous extract solutions by the method described in Rhoades (1982) using a solid to liquid ratio of 1:8 (2 g of subsample in 16 mL of water). pH and Eh were not determined in the extracts because they do not represent reliable environmental conditions regarding the actual cell system, but the method it is assumed to give a useful indicator for the content of soluble ions. Duplicates were made for all the samples. The distribution of exchangeable cations was determined in the different bentonite subsamples (D in Figure 3). A CsNO_3 solution was used to displace the exchangeable cations (Sawhney, 1970).

The samples remaining after soluble salt extraction from just subsamples labelled as D were used to extract the adsorbed iron. The method employed was a modification of the Aguilera and Jackson (1953) using 0.3M citric acid as extraction solution. This type of chelating agent removes only the more reactive sites of the clay surface, but does not dissolve either amorphous Fe oxides or magnetite/ilmenite. This fact is especially relevant as FEBEX bentonite contains up to 3% of amorphous Fe oxides and magnetite

1
2
3
4
5
6
7
8
9
10
11
12
13
14
15
16
17
18
19
20
21
22
23
24
25
26
27
28
29
30
31
32
33
34
35
36
37
38
39
40
41
42
43
44
45
46
47
48
49
50
51
52
53
54
55
56
57
58
59
60
61
62
63
64
65

271 was used in order to simulate the corrosion products layer in the tests. Neither
272 structural Fe nor exchangeable Fe is affected by citric acid, so it was assumed that Fe
273 determined by this method was mainly Fe absorbed in reactive surface sites of
274 montmorillonite.

275 2.5.2 Pore size distribution and BET specific surface area (SSA-BET)

276 The porosity and pore size distribution of bentonite samples, mortar and magnetite of
277 the samples labeled D was measured at the end of the tests by mercury intrusion
278 porosimetry (MIP) (Campos et al., 2013). Intact samples with respect to water content
279 and dry density were used after lyophilisation. The porosimeter used was a
280 Micromeritics AutoPore Series IV 9500, which applied a maximum injection pressure of
281 33000 psia (228 MPa), what allowed the exploration of pore sizes between 0.003 and
282 360 μm . The external specific surface area (SSA) was analyzed in the sections labeled U
283 in Figure 3, once they were dried under vacuum in a dry (P_2O_5) and CO_2 free
284 atmosphere, sampled and ground by hand in an agate mortar. 100-200 mg of these
285 samples were heated to 90 $^\circ\text{C}$ for 24 h in a sample holder and then outgassed in a
286 nitrogen current for 2h in a degasification station. The SSA was then determined by
287 nitrogen adsorption in combination with the BET equation in a Gemini V analyzer from
288 Micromeritics™ using the 5-points isotherm method.

289 2.5.3 Textural and elemental analyses at the interfaces

290 The sections labeled C in Figure 3 were prepared for embedding in LR-White© resin
291 following the procedure described by Cobeña et al. (1999) adapted from Kim et al.
292 (1995) to bentonite sections. Bentonite darkens with resin when it is not affected by

mortar alteration as can be globally observed in the whole Cell 6 with a single interface of magnetite (i.e. Figure 8). In contrast, a bright band of 4-5 mm characterizes the bentonite at the mortar interface for Cell 5 (Figure 3).

Textural and elemental analysis were performed by scanning electron microscopy (SEM) coupled with energy dispersive of X-rays detector (EDX). The study of the mineral morphologies and inter-relationships was performed in fresh fractured samples at the interfaces. Profiles of the chemical composition along the column axis were measured by SEM-EDX with a Hitachi S-3000N microscope and an INCAx-sight analyzer from Oxford Instruments.

2.5.4 Mineralogical analysis by X-ray Diffraction (XRD)

The XRD patterns registered from bulk randomly oriented powders and oriented < 2 μm aggregates were recorded in a $\theta/2\theta$ X-PERT Panalytical instrument with an X-CELERATOR detector (Cu K α monochromatic radiation). Patterns for iron rich minerals were recorded in a SIEMENS 5000 instrument with a solid state SiLi detector. Very small samples (< 50 mg) were taken at the interfaces or in special locations when the cells were dismantled. These powders were pressed with a spatula in a zero background ((111) surface) silicon wafer and then registered.

3 RESULTS

3.1 Water content and dry density

The 18th months experiments did not uptake water anymore after the two initial months, so they were fully saturated when the blocks were dismantled. Final dry

densities were similar in the different slices sampled in the bentonite material (± 0.02 g/cm³). However, the final water content and density behavior depended on the initial bentonite. Pretreated bentonite presented lower water content and higher dry density than the natural bentonite. The initial density of the bentonite (1.65 g/cm³) was maintained in the pretreated bentonite cells whereas decreased in natural bentonite tests (1.50 g/cm³) due to the bentonite expansion and the deformation of the Teflon[®] cell (see additional information file), without any evidence of cracking or leakage through the confining cell materials. The effect of partial dehydration of potassium at the interlayer induced by potassium exchange can be responsible for this different swelling behavior because the highest water content was achieved in natural bentonite either with or without mortar. In general, the absence of mortar produces a relative high final water content and low density in the pretreated bentonite cells.

3.2 Hydration water and distribution of soluble ions

A qualitative mass balance of soluble ions migration was made by using the initial and final composition of water in the reservoirs, and the initial and final soluble ions in the composite materials inside the cells. This approach was used for experiments 2 to 6 calculating the average values for the ions extracted in the different sections of the cell materials (Figure 4). The experiment corresponding to cell 1 was discarded due to an uncontrolled leakage during its dismantling.

There was a net two-way solute transfer between the cells and the hydration reservoir, at least for the initially more concentrated anions, chloride and sulfate. This means that the dimension of the cell tubing allowed for ion diffusion from the porous filter inside the cells. Chloride was lost from the bentonite with a net increase in the

hydration reservoir. However, cells with mortar allowed significant less chloride diffusion towards the reservoir. In contrast, sulfate and magnesium decreased in the reservoir although the magnitude was not matched with significant average increase inside the cells or to the presence or absence of mortar. For the cations, potassium increased in the reservoir and decreased in the pretreated bentonites (K-enriched), and calcium was extracted from the cells with mortar but was not perceptibly enriched in the reservoir. This indicates that calcium in these cells is mostly produced by the dissolution of portlandite or C-S-H in the water extracts used for determining soluble ions concentration. The behavior of sodium is complex and will be further described.

In order to explain the main aspects of soluble ions mobility, several coupled examples are presented using the data from soluble ions and exchangeable cations (see the complete data in the additional information files). The limited chloride diffusion from the cell towards the water-filled reservoir deposit or the decrease of sulfate in the water reservoir of cell 4, can be explained by the selective concentration of chloride in the mortar and the precipitation of sulfate solid phases, both in the mortar and in the magnetite powder (Figure 5). Additionally, chloride became depleted from the cell material and is back-diffused into the water reservoir when mortar is not present. This is deduced from the higher decrease in chloride in the cells without mortar which is also related to its highest increases in the corresponding water reservoirs.

The main counterion that balances major anions in solution (sulfate in hydration water and chloride in bentonite) is sodium, with the exception of the mortar material, in which the main counterion is calcium. Sodium can be supplied both by the hydration water or the exchange complex of the bentonite. In natural bentonite cells (cells 2 and

4 in Figure 6) there are minor changes in exchangeable sodium, but in the pretreated bentonite exchangeable sodium increased more than twice (up to 16 cmol(+)/kg) the initial value of 6.5 cmol(+)/kg, replacing mainly potassium that increase in soluble form, whereas calcium remains close to the initial values (cell 3 in Figure 6). This is in agreement with the decrease of sodium in the hydration water deposits of cells 5 and 6. Soluble sodium increased in the bentonites near the mortar interface and in the hydration water interface of both bentonites (natural and pretreated). The highest sodium increment occurs in the mortar-natural bentonite interface, where calcium has displaced all the magnesium and part of the sodium from the exchange complex. This effect can be also observed for magnesium in cell 3 (mortar-pretreated bentonite) and is indicative of the precipitation of M-S-H phases in the alkaline interface (Fernández et al., 2013). When comparing cell 1 and 2, without interfaces, it is interesting to note that soluble sodium concentration in the cell containing natural bentonite (cell 2) is double that in the cell with pretreated bentonite (cell 1), and the opposite occurs with potassium. The explanation for this observation is the above mentioned cation exchange process of sodium by potassium occurring in the pretreated bentonite.

The other focus of the chemical analyses done is determining the distribution of dissolved iron in the cells at the end of testing. The concentration of the total extracted iron along the columns ranged from a maximum value of 2.24 mmol/100g localized at section D1 in cell 3, which is adjacent to the interface with mortar, to background bentonite values (0.5 mmol/100g) or even lower concentrations at sections further away from hydration or the mortar interface including the magnetite interface. These data, SEM photos and a plot showing the distribution are provided in Figure 5. These data suggests that little magnetite was altered. Iron oxides were

observed to have precipitated from the hydration water at the bentonite-steel porous filter interfaces in the cells without mortar, but no visible corrosion was observed when alkaline conditions controlled by $\text{Ca}(\text{OH})_2$ solubility at 60 °C (pH 12.3) prevailed at the hydration source in contact with the steel elements facing the mortar disc. The alkaline environment of mortar therefore appears to provide steel with corrosion protection. The extractable iron maxima in the bentonite close to the mortar sections or at near the hydration source should be explained by means of the alteration of the initially present clay minerals or free oxides in the bentonite. These altered materials can better produce the release of soluble iron with the used reducing extraction method.

3.3 Porosity distribution and BET specific surface area (SSA BET)

Total intruded Hg porosity of natural bentonites (cells 2 and 4) is lower than total intruded porosity of pretreated bentonite (cells 1, 3, 5 and 6; compare 3 and 4 in Figure 7; see tables in additional information file). This can be related to higher water content and lower dry density of natural bentonite. This difference is caused by higher water adsorption in the smectite interlayers in natural than in pretreated, in which they are partially dehydrated or K^+ exchanged (less water molecules solvating the cation; i.e. Melkior et al., 2009). Water at the interlayers is located at the micropores (< 2 nm), which are not accessible to mercury intrusion and only partially accessible to N_2 gas (Rutherford et al., 2007). Then, the natural bentonite should contain a relative high proportion of small pores regarding the pretreated bentonite, which has a relative high population of mesopores (> 2 nm). On the other hand, sections of bentonite in

contact with mortar (named D1 in the three cells with mortar, 3, 4 and 5 (3 and 4 in Figure 7) have lower total Hg intruded porosity than sections outside the interface. The data show a similar trend in the three cells. The lowest values for total porosity near the mortar interface are in fact very similar to those for the initial bentonites. However, SSA BET values, more related to microporosity, decreased near the mortar. This is consistent with the existence of a microporosity sealing effect due to cementation and aggregation of particles, because the decrease of total Hg intruded could not be explained in this case by the presence of more expanded hydrated interfaces associated to the increase of microporosity. Moreover, if calcium dominates the exchange complex in this region a relative increase of SSA values should had been observed (Kaufhold et al., 2010).

3.4 Textural and elemental analysis at the interfaces

SEM-EDX characterization was focused to interfaces both in natural and pretreated FEBEX bentonite samples. Fresh fracture samples show a sharp contact between mortar and the bentonite. There were not morphological differences between the cells with pretreated bentonite (cells 3 and 5) or natural (cell 4) in the appearance of these interfaces. The interface with magnetite is not sharp as the compacted powder is slightly deformed when the compacted bentonite is pressed in the cell (Figure 8 d). New mineral phases, distinct of the original portlandite, have been produced during the hydration of mortar in contact with bentonite. The most frequent phase precipitated in the pore space of the mortar is calcium aluminum sulfate with needle morphology typical of ettringite (Figure 5). It has been remarked previously in this

paper that mortar acted as a sink for chlorides and sulfates. Although not related to new mineral morphologies, this is confirmed by the visible chloride content in the mortar matrix and the ubiquitous precipitates of sulfate in the mortar pores. In cell 4, near the interface it was possible to find also very low crystal size micellar or fibrous precipitates, rich in Mg silicates. Complementary to these precipitation processes it is relevant the precipitation of gypsum needles and brucite aggregates at the hydration source-mortar interfaces (see details in additional information files).

Several backscattering (BSE) mode SEM images have been used to build a reconstruction of the interface zones of cells 3, 4, 5 and 6 (Figure 8). Near the bentonite interface, the mortar matrix tends to darken, what it is indicative of the dissolution of the matrix as a consequence of Ca loss and low energy dispersivity in the zone. The bentonite behind the mortar forms a compact rim which further ended in a break parallel to the interface, produced after this mortar-bentonite alteration band. From this zone the bentonite has a granular aspect due to the subtle shrinkage of smectite grains during sample preparation. The micro-cracks in the alteration band and the absence of retraction indicate a material consistency more brittle than a plastic. This band was less developed in cell 4 (Figure 8b). The cracks in this sample could be exaggerated because of the mechanical damage suffered during cutting (see additional information files).

Attending to the aspect of the mortar, the matrix darkens in cell 4 with more extension, and this dark zone often faces to preferential paths that end in micro-crack

propagation direction towards the bentonite. This can indicate preferential sources of alkaline alteration in zones where portlandite would be dissolved to a greater extent.

In contrast to the alkaline interface, the magnetite interface, shown in Figure 8d for cell 6, did not show any special textural process development apart from the mechanical mixing of magnetite powder grains. This agrees with the lack of any migration front of Fe towards the bentonite at the magnetite interface (see details of iron profiles in the interface zone in the additional information file).

The alkaline mortar interface is characterized by the development of a calcium front towards the bentonite. Calcium in mortar is dissolved near the bentonite interface in the three mortar interfaces studied in cells 3, 4 and 5 (Figure 9, upper part). Regarding the plateau at 5 weight % Ca in the bentonite, a relative increase of calcium from 10 mm until the interface is observed, being the affected thickness around 4 mm in pretreated bentonite cells (3 and 5) and 1.5 mm in natural bentonite (cell 4). A magnesium maximum marks the end of the calcium front. This maximum indicates presumably the precipitation of magnesium silicate hydrates (MSH), which seems to buffer the accumulation of calcium. Pretreated bentonite has minor quantities of exchangeable magnesium and the precipitation front of MSH is not significantly produced. In turn, potassium is visible in cell 3 and not in cell 4 (K is virtually absent from the exchange complex). Aluminum follows the opposite trend of calcium and accumulates in small amounts in the first 1-2 mm in the mortar near the bentonite-mortar interface (cells 3, 4 and 5). This is also related to the increase of sulfur (Figure 9, lower part) in agreement with the presence of ettringite-like needles. Chloride and

sodium have less consistent trends and sensitivity in the analyses and did not exhibited significant trends in the chemical line profiles.

3.5 Mineralogy

Previous results, described above, put the evidence of a 1-5 mm thickness bentonite alteration band in contact with the lime mortar. This band is characterized by a small capacity to absorb the embedment resin, a low N₂ adsorption specific surface, a relative low intruded Hg porosity (compared to bentonite outside the mortar influence), and also by becoming compact and brittle. Besides, the study of chemistry shows a significant redistribution of calcium and magnesium, produced by the dissolution of portlandite in the mortar or by magnesium exchange, mostly in the natural bentonite. In contrast, magnetite seems not to produce such extent of alteration effects. Magnetite XRD patterns reveal minor alterations in the material. Just small evidence of Fe(II) carbonate (siderite) presence and iron oxidation (hematite traces) could be observed (see detail in additional information files). These three phases may coexist in equilibrium under very specific conditions (close to pH 7, Eh -0.25 V at 75 °C; Chivot (2004), which are reasonably consistent with those expected in this type of experiment.

The dissolution of portlandite in the mortar that was in contact with bentonite represent approximately the half of the initial portlandite, which became severely dissolved in all the experiments. This is observed by the decrease in the area of the 4.90 Å d-spacing peak, in the mortar patterns, in the middle section of the Figure 10 (a semi-quantitative data set for these XRD patterns is provided in the additional information file). Despite of the identification of ettringite-like phases in the mortar

pores, they were difficult to identify in the XRD patterns. Very small reflections characteristic of AFm-like phases like monosulfates or carboaluminates were found rather than ettringite. It is possible that the sulfate-rich rim (<0.5 mm in Figure 9) has represented a thin part of the altered mortar which was not possible to be properly sampled for XRD inspection.

The mineralogical representation of the calcium front developed towards the bentonite is evidenced by the presence of C-S-H phases of tobermorite type (Fernández et al., 2014). These phases have very low crystal size and can be detected by the presence of a 3.08 Å broad reflection visible in D1 sections in samples of cells 3 and 5 in Figure 10. The relative intensity of 3.08 Å C-S-H reflection to the 3.03 Å calcite reflection is significantly higher in the pretreated bentonite cells, which is in agreement with the extended calcium accumulation in these cells and clearly visible in the C-S-H and calcite presence in cell 5 up to 3mm from the interface (C5D1 9mm).

X-ray powder patterns of bentonites after the experiments in cells with no interfaces are very similar to the originally emplaced bentonites (Figure 10, upper part). The first reflection in the region near $6^\circ 2\theta$ (14-15 Å spacings) corresponding to the basal spacing of smectite (001 hkl Miller indexes or the repeating distance **c** between interlayers) remained within the values described in the materials section. These patterns show the very similar wt% estimation (> 90 % smectite) for all the bentonite samples, with or without interfaces. The 060 (1/6 of the repeating distance in the **b** dimension) reflections are slightly displaced from natural to pretreated bentonite samples (1.500 to 1.501 Å).

The bentonite samples near the mortar in the cells 3, 4 and 5 show a 12-12.5 Å for the first reflection of the basal spacing (Figure 10 lower part, D1 samples), which is a very small value taking into account the presence of calcium in the smectite (commonly 15 Å). These reflections are very broad and overlap with the angles at which some C-S-H of tobermorite type (14-11-9 Å type) can be observed. Then, the low angle reflection of this region can be interpreted to be consistent with a mixture of clay and C-S-H phases. The bentonite samples in the magnetite contact have no evidence of any discernible alteration (D3 sample).

The clays at the mortar interface have been extracted (< 2µm fraction was separated by dispersion and sedimentation), oriented and EG-solvated all in absence of CO₂. They showed broad reflections because it was difficult to perform the standard orientation procedure on this type of material. Specifically, they do not have the same dispersability as the non-60 °C heated bentonite. However, they exhibited smectite typical expansion. As it was mentioned previously in this paper, pretreated bentonite was observed to have partially collapsed following pretreatment, but this collapse was reversed during the experiment by calcium exchange because smectite expands with EG to an apparently higher smectite content (80 % smectite versus 60%) than the initial pretreated (heated or not, see Figure 1) bentonites (see profiles in additional information files). Finally, bentonite outside the influence of the mortar interface has developed a double basal spacing reflection at 14.8 Å (calcium) and 13.8 Å (calcium-potassium); (see C5D3 in lower part of Figure 10). This means that some of the interlayers have apparently taken up more calcium than others in the interaction with the calcium front.

543

544 **4. Discussion**

545 The small scale experiments were planned with an intent to examine conditions that
546 might be present in a mid-long term (1-10 ky) time window after emplacement of the
547 waste in the DGR. One of the goals of this paper is to discuss how an aged bentonite in
548 contact with concrete or iron corrosion products will be affected. The study focuses on
549 the geochemical response of the each component and of the whole system. This will
550 allow for evaluation of the resulting effects on the physical-chemical properties and by
551 extension the hydro-mechanical functionality of the clay barrier.

552 The starting point for this was the preparation of the aged bentonite itself. An alkaline
553 concrete (i.e., high pH CEM-I) will force the calcium and potassium exchange in the
554 bentonite and the displacement and precipitation of Mg bearing phases (Brucite, M-S-
555 H). Both processes have previously been identified or observed in experiments and
556 considered in modelling exercises (Gaucher et al., 2004; Cuevas et al., 2006; Yang et
557 al., 2008; Fernández et al., 2009, Samper et al., 2010; Fernández et al., 2013). The Ca-K
558 exchanged aged bentonite was prepared by soaking it in neutral chloride solutions,
559 avoiding the presence of M-S-H, which precipitates at pH 10-11 (Zhang et al., 2011), in
560 the aged material. The Ca exchange does not cause any alteration in the layer
561 structure of montmorillonite under hydrothermal conditions up to 120 °C (Sánchez et
562 al., 2006; Fernández et al., 2009). However, the partial K exchange at ambient
563 temperature, although not anticipated to mimic aged conditions, caused dehydration
564 of some montmorillonite interlayers. This collapse behavior was used in early clay
565 characterization methodology as indicative of high charge montmorillonite-beidellite

presence (Malla and Douglas, 1987) and has been produced also in montmorillonite hydrothermal reactions (Mosser-Ruck et al., 2001, Mosser-Ruck and Cathelineau, 2004). Then, the term “aged” for the prepared pretreated bentonite could be justified by two aspects: (1) the absence of exchangeable-Mg due to previous alkaline impact and (2) the potential time-dependent (long-term) illitization of the bentonite. This later effect has been argued to be not realistic during the time span of the DGR activity and the Thermal, Pressure conditions ($< 100^{\circ}\text{C}$, $< 1\text{ kbar}$; Wersin et al., 2007). The possibility of having a partial dehydration is however evidenced in the current work, although with the recognized limitation of the present K availability.

Regarding the interface materials, magnetite behaved as a stable product under this virtually closed system environment as deduced from various previous experimental studies (Guillaume, 2004; Wersin et al., 2008; Torres et al., 2011, 2013) in agreement with thermodynamic data (Chivot, 2004). This earlier information is consistent with the study described in this paper. Very small Fe penetration front into the bentonite, less than 0.1 mm, is presumably due to mechanical mixing of bentonite and the magnetite powder. In contrast, the use of lime mortar is not a perfect analogue for aged cement matrix as far as carbonation (Tinseau et al., 2006) or the initial formation of low Ca/Si C-S-H phases in the cement matrix (Dauzeres et al., 2010) were not considered.

Although not entirely representative, in order to have an active calcium source and to test the long-term alkaline impact on the different studied materials “aged” or pristine “natural” bentonite, the approach taken in this study was deemed to be appropriate.

The use of aged (pretreated) or natural bentonite in the experiments determined the final dry density and hence the water content at saturation; the C-S-H front migration

in the bentonite; and also the mode of anions migration in the system, although the last was strongly influenced by the presence of mortar and magnetite. The case of chloride discriminates different transport behavior caused by initial qualities of the bentonite. In the cell 1 containing pretreated bentonite, the chloride concentration is higher in the section closer to hydration source (0.4 mmol/100g) than in the rest of the sections, where values are close to 0. However, it is quite homogeneous (≈ 0.3 mmol/100g) along the bentonite column in cell 2 containing natural bentonite. In any case, chloride values are very low compared with the original value in FEBEX bentonite (see Table IV), which can be justified by two facts: (1) a back-diffusion process occurring from the cells towards the hydration bottle once bentonite is saturated, a phenomenon observed in other experiments (Buil et al., 2010), and (2) by the exclusion of chloride in the high density-lower water content at saturation observed in the pre-treated bentonite. It is known that at 1.6 g/cm^3 dry densities or beyond, as in the case of cell 1, 1-2 interlayer cation-water complexes dominate the global water content in compacted bentonite, which decreases critically the accessible porosity for anions in the system (Van Loon et al., 2007; Tournassat and Appello, 2011). Cell 6 also contains pretreated bentonite, but the porous magnetite powder at the opposite side of the hydration source allows the bentonite to swell achieving relative lower dry densities presumably located close to the magnetite interface. This porous layer also acted as a sink for chloride. This anion was not solely diffused from the bentonite plug towards the hydration reservoir ($\approx 0.5 \text{ mmol/100g}$) but to the magnetite porous layer. In the cells 3, 4 and 5 the distribution of chloride concentration is tied to the concentration of saline fronts of chloride moving towards mortar and/or magnetite. The back diffusion of chlorides towards the hydration reservoir did not occur at the

same level in these cells as they were for those without interfaces. This is in agreement with the observed chloride retention in the mortar matrix. As the materials become fully saturated the transfer of chlorides by concentration gradient or anion exclusion in the pore solution of the different materials occurs. The mortar can react with chloride in different ways to form chloroaluminates or Friedel's salt as Afm-like phases, or adsorbed in C-S-H minerals (Baur et al., 2004; Yuan et al., 2009; Florea and Browers, 2012), thus retaining the chloride at mortar mineral surfaces and decreasing the concentration of free chloride ions in the pore solution. The presence of Afm phases as carboaluminate and C-S-H has been detected in small quantities by XRD measurements and chloride can be analyzed in the mortar matrix (no distinguishable crystal morphologies). This could be the reason for the lower concentration of chloride in the final hydration water of the dismantled cells with mortar (Figure 8) and the sharp increase of aqueous extractable chloride at the mortar sections (see Table IV). Sulfate shows very similar behavior to that of chloride in cells containing mortar interfaces. In this case ettringite-like (Aft) needle aggregates were clearly observed in mortar pores by SEM-EDX, but not detected by XRD. Afm monosulfate used to be part of the cement matrices or pastes and ettringite precipitates in pores when it is formed after the hardening of cement. This precipitation can cause undesired expansion effects (sulfate attack) (Menéndez et al., 2013). The last was not observed in our mortars, presumably due to the extensive dissolution of portlandite creating pore space for secondary minerals precipitation. It comes evident, from the sentences above, that a more detailed solubility equilibrium study, focused to thermodynamic validation of the precipitation of these phases in the mortar-bentonite interface, will be further needed.

The diffusive transport of solutes across a cement-clay interface leads to sharp gradients in pH and $p\text{CO}_2$, which become fixed as solid carbonate and regulated to very low activities under the cement alkaline medium. Such sharp gradients encourage rapid precipitation of carbonates, hydroxides and C-S-H or M-S-H phases, leading to decreased porosity (e.g. Watson et al., 2009). Fast protonation-deprotonation reactions at clay edge sites can typically neutralise 55 moles of hydroxyl ions per cubic metre of MX-80 bentonite (at 2000 kg m⁻³ water-saturated compaction density; Savage et al, 2007). In addition, montmorillonite and other minerals present, such as cristobalite, quartz and feldspars can be dissolved to some extent at high pH (Marty et al., 2015). Such reactions consume hydroxyl ions and slow down the progress of the high pH front. The proof of the dissolution of these minerals is the presence Al (Aft or Afm) or Mg (M-S-H) phases which were not initially contained in the lime mortar that, in turn, indicate reaction and mass transfer processes coming from the bentonite material. Tobermorite-like (low Ca/Si) C-S-H and calcite determined in the mortar of cells 3 and 5 reflect also the diffusive transport of dissolved silica and carbonate species from the bentonite to the alkaline mortar material.

Both Dauzères et al., (2014) or Jenni et al. (2014) have shown recently, in real low pH or high pH concrete interfaces, the significance of carbonation and sulfate phases dynamics in producing porosity changes. Dissolution-precipitation and the associated clogging fronts of calcite (both in concrete and clay) or new precipitation of ettringite (concrete) in < 1 mm depth, will favor the isolation of local equilibrium compartments as far as the porosity will be reduced locally, which stops or slow down further mineralogical alteration. These cementing processes are more active in high pH OPC than low pH OPC. Then, the slow solutiontransport and hence the lower grade in

mineralogical alteration might prevent the complete reaction of OPC concrete with bentonite (Savage et al., 2010). Of course this aspect will be better known as long as several in situ long-term (i.e. 15-20 years) experiments with real interfaces can be studied (Soler, 2013).

Related to the neutralization of the high-pH front, cation exchange reactions also take place. The most significant reaction is the drastic magnesium depletion mainly counteracted by calcium exchange, registered in the whole 18 mm length of bentonite in cell 4 (mortar and magnetite interfaces with natural bentonite). This is produced by the precipitation of Mg hydroxides and/or silicates known to take place at > pH 10-10.5. A sharp Mg gradient is created because precipitated M-S-H is concentrated in a narrow delimited space at 1-1.5 mm from the interface collecting all the exchanged Mg in the bentonite specimen. When exchangeable Mg was not present (pretreated bentonite cells), calcium exchange was less significant and C-S-H phases formed up to 3-4 mm from the mortar interface. According to these experimental results, Mg-exchanged natural bentonite has potentially a buffer capacity to attenuate the calcium alkaline front and to produce a delay in the C-S-H formation processes between both materials, due to Mg reactivity and M-S-H precipitation (Cuevas et al., 2014).

4 Conclusion

The experimental study presented in this paper provides evidence of a potential variety of mass transfer processes occurring in the EBS of a DGR taking in mind a simplified experimental setup which tried to mimic the repository conditions prevailing from 1000 to 3000 years after emplacement. Among all the identified processes the

most important are; (a) influencing chloride and sulfate transport in the “formation porewater-mortar-bentonite-magnetite” system; b) the cation exchange processes and (c) the precipitation of carbonates, hydroxides, and C-S-H, M-S-H and Aft (or Afm) phases, mainly in the mortar-bentonite interface.. Related to the last item listed above, the mass transfer induced by mineral dissolution/precipitation determines variations in the porosity of the medium. No significant reaction processes were identified at the bentonite-magnetite interface, presumably caused by thermodynamic solubility constrains.

The main outcomes relevant for clay barrier performance are: (1) the potential capacity of concrete interfaces to act as a sink of soluble salts (chlorides and sulfates), coming from the clay formation porewater or migrated through the bentonite, which may contribute to partially prevent further corrosion processes towards the metallic canister (corrosion will be enhanced by chlorides); and (2) the positive role of exchangeable Mg buffering capacity regarding the partial neutralization of an alkaline plume. On the other hand, regarding the performance analogue of the “aged” bentonite, two undesirable physical-chemical effects were identified, presumably valid for the most common Na-Ca bentonites. These can have negative consequences at long-term for the hydro-mechanical performance of the clay barrier near the concrete interface. The first is the K^+ exchange and the second is bentonite porosity decrease when C-S-H-like phases precipitate. The availability for exchangeable K^+ that could be uptaken from cementitious materials, affecting initially the bentonite hydration and swelling, needs to be evaluated precisely in high pH OPC cements in order to ascertain this effect. Finally, mostly related to the mortar (concrete) interface, where a low porosity bentonite zone was created in the experiments done in this study. This should

1
2
3
4
5
6
7
8
9
10
11
12
13
14
15
16
17
18
19
20
21
22
23
24
25
26
27
28
29
30
31
32
33
34
35
36
37
38
39
40
41
42
43
44
45
46
47
48
49
50
51
52
53
54
55
56
57
58
59
60
61
62
63
64
65

707 be carefully studied in order to evaluate either the sealing effect for ions, and hence
708 RN transport, or the consequences in decreasing the hydration rate of the bentonite
709 and the retardation of the development of the swelling capacity of the whole system.
710 This issue needs to be considered as part of evaluation of dismantling of long-term real
711 interface experiments in the future.

712 **Acknowledgements**

713 The research leading to these results has received funding from the European Atomic
714 Energy Community's Seventh Framework Program (FP7/2007-2011) under grant
715 agreement nº 249681.

716 We would to thank to Nicolas Michau for his very valuable effort in comments and to
717 an anonymous referee who has improved discussion and the quality of the text.

719 **References**

- 720 Adler, M., Mäder, U.K., Waber, H.N., 1999. High pH alteration of argillaceous rocks: an
721 experimental study, Schweizerische Mineralogische und Petrographische Mitteilungen,
722 79, 445–454.
- 723 Aguilera N.H., Jackson M.L., 1953. Iron Oxide Removal from Soils and Clays. Soil Sci.
724 Soc. Am. J. 17, 359–364.
- 725 Bäckblom, G. (2005). R&D on low-pH cement for a geological repository. 2nd low-pH
726 workshop proceedings. Madrid, June 15-16, 2005. Enresa, SKB and the ESDRED-
727 project. 200pp.
- 728 Baur, I., Keller, P., Mavrocordatos, D., Wehrli, B., Johnson, C.A. 2004. Dissolution-
729 precipitation behaviour of ettringite, monosulfate, and calcium silicate hydrate.
730 Cement and Concrete Research, 34, 341–348.
- 731 Berner, U., Kulik, D. and Kosakowski, G. 2013. Geochemical impact of a low-pH cement
732 liner on the near field of a repository for spent fuel and high-level radioactive waste.
733 Physics and Chemistry of the Earth, 64, 46–56.

734 Blake, CR. and Hartge, K.H., 1986. Bulk density. In: Methods of soil analyses Part 1, 2nd
 735 edition. Ed. A. Klute. Agron. Monogr. 9. ASA and SSSA, Madison. WI. p. 363-375.
 736 Buil, B., Gómez, P., Peña, J., Garralón, A., Turrero, M.J., Escribano, A., Sánchez, L.,
 737 Durán, J.M. (2010): Modelling of bentonite–granite solutes transfer from an in situ full-
 738 scale experiment to simulate a deep geological repository (Grimsel Test Site,
 739 Switzerland). *Applied Geochemistry*, 25, 1797–1804.
 740 Caballero, E., Jiménez de Cisneros, C., Huertas, F.J., Huertas, F., Pozzuoli, A., Linares, J.,
 741 2005. Bentonite from Cabo de Gata, Almería, Spain: a mineralogical and geochemical
 742 overview. *Clay Miner.* 40, 463–480.
 743 Campos, R., Barrios, I. González, A.M. 2013. Estudio de la porosidad en las Celdas C1 a
 744 C6: procesos de de corrosión/alteración en condiciones saturadas. Informe Técnico
 745 CIEMAT/DMA/2G210/6/13. 108 pp.
 746 Chivot, J. 2004. Thermodynamique des produits de corrosión. Fonctions
 747 thermodynamiques, diagrammes de solubilité, diagrammes E-pH des systèmes Fe-
 748 H₂O, Fe-CO₂-H₂O, Fe-S-H₂O, Cr-H₂O et Ni-H₂O en fonction de la température. Colle-
 749 tion Sciences & Techniques. Andra - Février 2004 - IBSN 2-9510108-6-9, 140 pp.
 750 Claret, F., Bauer, A., Schafer, T., Griffault, L., Lanson, B. 2002. Experimental
 751 Investigation of the interaction of clays with high-pH solutions: a case study from the
 752 Callovo– Oxfordian formation, Meuse-Haute Marne underground laboratory (France),
 753 *Clays and Clay Minerals*. 50, 633–646.
 754 Cobeña, J., Cuevas, J., Martín, M., Ramírez, S., Vigil de la Villa, R. and Leguey, S. 1999.
 755 Estudio de la mineralogía y microestructura de una bentonita compactada. Efectos de
 756 calentamiento e hidratación. *Boletín de la Sociedad Española de Mineralogía*, 22, 235-
 757 247.
 758 Cuevas, J., Vigil de la Villa, R., Ramírez, S., Sánchez, L., Fernández, R., and Leguey, S.
 759 2006. The alkaline reaction of FEBEX bentonite: a contribution to the study of the
 760 performance of bentonite/concrete engineered barrier system. *Journal of Iberian*
 761 *Geology*. 32 (2), 151-174

762 Dauzères, A., Le Bescop, P., Sardini, P., Cau-Dit-Coumes, C. 2010. Physico-chemical
 763 investigation of clayey/cement-based materials interaction in the context of geological
 764 waste disposal, experimental approach and results, *Cem. Concr. Res.* 40, 1327–1340.
 765 Dauzères, A., Le Bescop, P., Cau-Dit-Coumes, C., Brunet, F., Bourbon, X., Timonen, U. J.,
 766 Voutilainen, M., Chomat, L., Sardini, P. 2014. On the physico-chemical evolution of
 767 low-pH and CEM I cement pastes interacting with Callovo-Oxfordian pore water under
 768 its in situ CO₂ partial pressure *Cement and Concrete Research*. 58, 76–88.
 769 Devol-Brown, I., Tinseau, E., Bartier, D., Mifsud, D., Stammose, D. 2007. Interaction of
 770 Tournemire argillite (Aveyron, France) with hyperalkaline fluids: batch experiments
 771 performed with powdered and/or compact materials, *Physics and Chemistry of the*
 772 *Earth*, 32, 320–333.
 773 ENRESA. 2004. Evaluación del comportamiento y de la seguridad de un almacén
 774 geológico profundo de residuos radiactivos en arcilla. Clave: 49–1PP-M-A1–01. ENRESA
 775 (in Spanish).
 776 ENRESA. 2006. FEBEX Full-scale Engineered Barriers Experiment, Updated Final Report
 777 1994-2004. Publicación Técnica ENRESA 05-0/2006, Madrid, 590 pp.
 778 Fernández, R., Cuevas, J., Mader, U. 2009. Modelling concrete interaction with a
 779 bentonite barrier. *Eur. J. Mineral.* 21, 177–191.
 780 Fernández, R., De la Villa, R., Ruiz, A.I., García, R. and Cuevas, J. 2013. Precipitation of
 781 chlorite-like structures during OPC porewater diffusion through compacted bentonite
 782 at 90 °C, 83–84, 357–367.
 783 Fernández, R., González, L., Ruiz, A.I., Cuevas, J. (2014). Nature of C-(A)-S-H Phases
 784 Formed in the Reaction Bentonite/Portlandite. *Journal of Geochemistry*. Volume 2014,
 785 Article ID 145425, 8pp.
 786 Fernández, R., Mäder, U.K., Rodríguez, M., Vigil de la Villa, R., Cuevas, J., 2009.
 787 Alteration of compacted bentonite by diffusion of highly alkaline solutions. *European*
 788 *Journal of Mineralogy* 21, 725–735.
 789 Florea, M.V.A., Brouwers, H. J. H. 2012. Chloride binding related to hydration products
 790 Part I: Ordinary Portland Cement / *Cement and Concrete Research*, 42, 282–290.

791 Garcia Calvo, J.L., Hidalgo, A., Alonso, C., Fernandez Luco, L. 2010. Development of
792 low-pH cementitious materials for HLRW repositories: resistance against ground
793 waters aggression, *Cem. Concr. Res.* 40, 1290-1297.

794 Gaucher, E. C., Blanc, P. 2006. Cement/clay interactions - A review: Experiments,
795 natural analogues, and modeling. *Waste Management*, 26, 7, 776-788.

796 Gaucher, E.C., Blanc, P., Matray, J.M., Michau, N. 2004. Modeling diffusion of an
797 alkaline plume in a clay barrier, *Applied Geochemistry*, 19, 1505–1515.

798 Gaucher, E.C., Tournassat, C., Pearson, F.J., Blanc, P., Crouzet, C., Lerouge, C., Altmann,
799 S. 2009. A robust model for pore-water chemistry of clayrock, *Geochimica et*
800 *Cosmochimica Acta*, 73, 6470-6487.

801 Guillaume, D., Neaman, A., Cathelineau, M., Mosser-Ruck, R., Peiffert, C., Abdelmoula,
802 M.; Dubessy, J., Villi  ras, F., Michau, N. 2004. Experimental study of the transformation
803 of smectite at 80 and 300  C in the presence of Fe oxides. *Clay Minerals*, 39, 17-34.

804 Jenni, A., M  der, U., Lerouge, C., Gaboreau, S., Schwyn, B. 2014. In situ interaction
805 between different concretes and Opalinus Clay. *Physics and Chemistry of the Earth*,
806 70-71, 71-83

807 Kaufhold, S., Dohrmann, R., Klinkenberg, M., Siegesmund, S. and Ufer, K. 2010. N2-BET
808 specific surface area of bentonites. *Journal of Colloid and Interface Science*, 349, 1,
809 275-282.

810 Kim, J., Peacor, D., Tessier, D. and Elsass, F. 1995. A technique for maintaining texture
811 and permanent expansion of smectite interlayer for TEM observations. *Clays and Clay*
812 *Minerals*, 43, 51-57.

813 King, F., Kol  ř, M., Keech, P.G. 2014. Simulations of long-term anaerobic corrosion of
814 carbon steel containers in Canadian deep geological repository. *Corrosion Engineering,*
815 *Science and Technology*, 49, 455-459.

816 Leguey, S., Cuevas, J., Ram  rez, S., Vigil de la Villa, R., Mart  n-Barca, M. 2002. Alteraci  n
817 alcalina hidrot  mal de la barrera de bentonita por aguas intersticiales de cementos.
818 ENRESA publicaci  n t  cnica 03/2002. 171pp.

819 Malla, P. B. and Douglas, L. A. 1987. Identification of expanding layer silicates: Layer
820 charge vs. expansion properties: in Proc. Int. Clay Conf., Denver, L. G. Schultz, H. van
821 Olphen, and F. A. Mumpton, eds., 277-283.

822 Marty, N.C.M., Claret, F., Lassin, A., Tremosa, J., Blanc, P., Madé, B., Giffaut, E.,
823 Cochevin, B., Tournassat, C., 2015. A database of dissolution and precipitation rates for
824 clay-rocks minerals. *Applied Geochemistry*, 55, 108-118.

825 Melkior, T., Gaucher, E.C., Brouard, C., Yahiaoui S., Thoby, D., Clinard, Ch., Ferrage, E.,
826 Guyonnet, D., Tournassat, C., Coelho, D. 2009. Na⁺ and HTO diffusion in compacted
827 bentonite: Effect of surface chemistry and related texture. *Journal of Hydrology*, 370,
828 9–20.

829 Menéndez, E., Matschei, T. and Glasser, F.P. 2013. Sulfate attack of Concrete. In:
830 Performance of Cement-Based Materials in Aggressive Aqueous Environments State-
831 of-the-Art Report, RILEM TC 211 – PAE Series: RILEM State-of-the-Art Reports, Vol. 10.
832 Alexander, Mark, Bertron, Alexandra, De Belie, Nele (Eds.) 2013, XVI, Springer 462, 7-
833 71.

834 Montes-H, G., Marty, N., Fritz, B., Clement, A., Michau, N. 2005. Modelling of long-
835 term diffusion–reaction in a bentonite barrier for radioactive waste confinement
836 *Applied Clay Science* 30, 181 – 198

837 Moore, D.M., Reynolds, R.C., 1997. X-Ray Diffraction and the Identification and
838 Analysis of Clay Minerals, 2nd ed. Oxford University Press, New York. 378 pp.

839 Mosser-Ruck, R., Pironon, J., Cathelineau, M., Trouiller, A., 2001. Experimental
840 illitization of smectite in a K-rich solution. *Eur. J. Mineral.* 13, 829 – 840.

841 Mosser-Ruck, R., Cathelineau, M., 2004. Experimental transformation of Na,Ca-
842 smectite under basic conditions at 150 °C. *Applied Clay Science*, 26, 259 – 273.

843 NEA-OECD. 2003. Engineered Barrier Systems and the Safety of Deep Geological
844 Repositories. State-of-the art Report. OECD Publications, Paris. 70pp.

845 Plançon, A., Drits, V.A., 2000. Phase analysis of clays using an expert system and
846 calculation programs for X-ray diffraction by two- and three-component mixed-layer
847 minerals. *Clays Clay Miner.* 48, 57–62.

848 Rhoades, J.D., 1982. Soluble salts. In: Methods of soil analysis Part 2, 2nd edition. Ed.
 849 A. Klute. Agron. Monogr. 9, American Society of Agronomy. Madison, pp. 167-179.
 850 Rutherford, D.W., Chiou, C.I., and Eberl, D.D. (1997). Effects of exchanged cation on
 851 the Microporosity of montmorillonite. *Clays and Clay Minerals*, 45, 534-543.
 852 Samper, J., Montenegro, L., Turrero M.J., Martín, P.L., Garralón, A., Cuevas, J. and
 853 Fernández, R. 2010. Technical Note 1: Design of new experiments. PEBS Internal
 854 Deliverable D 3.4.2. 10 pp.
 855 Sánchez, L., Cuevas, J., Ramírez, S., Ruiz de León, D., Fernández, R., Vigil de la Villa, R.,
 856 Leguey, S., 2006. Reaction kinetics of FEBEX bentonite in hyperalkaline conditions
 857 resembling the cement–bentonite interface. *Appl. Clay Sci.* 33, 125–141.
 858 Santhanam, M. 2013. Magnesium attack of concrete in marine environments. In:
 859 Performance of Cement-Based Materials in Aggressive Aqueous Environments State-
 860 of-the-Art Report, RILEM TC 211 – PAE Series: RILEM State-of-the-Art Reports, Vol. 10.
 861 Alexander, Mark, Bertron, Alexandra, De Belie, Nele (Eds.) 2013, XVI, Springer. 76-90.
 862 Savage, D., Walker, C., and Benbow, S. 2010. An Analysis of Potential Changes to
 863 Barrier Components due to Interaction with a Concrete Liner in a Repository for
 864 SF/HLW in Opalinus Clay. NAB 10-17. Nagra report. 39 pp.
 865 Savage, D., Walker, C., Arthur, R., Rochelle, C., Oda, C. and Takase, H. 2007. Alteration
 866 of bentonite by hyperalkaline fluids: A review of the role of secondary minerals.
 867 *Physics and Chemistry of the Earth, Parts A/B/C*, 32, 1-7, 287-297.
 868 Sawhney B.L., 1970. Potassium and cesium ion selectivity in relation to clay mineral
 869 structure. *Clays and Clay Minerals*. 18, 47-52
 870 Smart, N.R., Blackwood, D.J., Werme, L. 2002. Anaerobic Corrosion of Carbon Steel and
 871 Cast Iron in Artificial Groundwaters: Part 1—Electrochemical Aspects. *Corrosion*, 58,
 872 547-559.
 873 Soler, J.M. 2013. Reactive transport modeling of concrete-clay interaction during 15
 874 years at the Tournemire Underground Rock laboratory. *European Journal of*
 875 *Mineralogy*, 25, 639-654.

876 Tinseau, E., Bartier, D., Hassouta, L., Devol-Brown, I., Stammose, D. 2006. Mineralogical
 877 characterization of the Tournemire argillite after in situ interaction with concretes,
 878 Waste Management. 26, 789–800.

879 Stefanidou, M. and Papayianni, I. 2005. The role of aggregates on the structure and
 880 properties of lime mortars. Cement & Concrete Composites. 27, 914–919.

881 Techer, I., Bartier, D., Boulvais, Ph., Tinseau, E., Suchorski, K., Cabrera, J., Dauzères, A.
 882 2012. Tracing interactions between natural argillites and hyper-alkaline fluids from
 883 engineered cement paste and concrete: Chemical and isotopic monitoring of a 15-
 884 years old deep-disposal analogue. Applied geochemistry. 27, 1384–1402.

885 Torres, E., Turrero, M.J., Escribano, A., Martín, P.L. 2013. Formation of iron oxide and
 886 oxy-hydroxides under different environmental conditions: Iron/bentonite interaction.
 887 Deliverable D2.3-6-2 of Project “Long-term Performance of Engineered Barrier
 888 Systems” (http://www.pebs-eu.de/PEBS/EN/Home/PEBS_node_en.html)

889 Torres, E. 2011. Geochemical processes at the C-steel/bentonite interface in a Deep
 890 Geological Repository: experimental approach and modelling. UCM. PhD Thesis.

891 Torres, E., M.J. Turrero, P.L. Martín. 2007. Geochemical processes at the Carbon
 892 Steel/bentonite interface in repository conditions. Sci. Basis Nuclear Waste Manag.-
 893 Mat. Res. Soc. Symp. Proc. Editors: Dunn D; Poinssot C; Begg B. 985, 569-574.

894 Tournassat, C., Appelo, C.A.J. 2011. Modelling approaches for anion-exclusion in
 895 compacted Na-bentonite. Geochimica et Cosmochimica Acta. 75, 3698–3710.

896 Turrero, M.J., Fernández, A.M., Peña, J., Sánchez, M.D., Wersin, P., Bossart, P.,
 897 Sánchez, M., Melón, A., Yllera, A., Garralón, A., Gómez, P., Hernán P. 2006. The pore
 898 water geochemistry of Paleogene continental mudrocks in Spain and Jurassic marine
 899 mudrocks in Switzerland: sampling methods and geochemical interpretation. Journal
 900 of Iberian Geology. 32(2), 233-258.

901 Turrero, M.J., Peña, J., Fernández, A.M., Gómez, P., Garralón, A. 2001. Porewater
 902 geochemistry and modeling within Oligocene-Miocene Clays of North-Central Spain.
 903 Proceedings of the tenth international symposium on Water-Rock Interaction. R. Cidu
 904 (ed.) Balkema, Rotterdam. ISBN 90-2651-835-8. 1, 213-216.

905 U.S. Department of Energy. 2014. Evaluation of Options for Permanent Geologic
 906 Disposal of Spent Nuclear Fuel and High-Level Radioactive Waste, Volume I. Used Fuel
 907 Disposition Campaign. Sandia National Laboratories. FCRD-UFD-2013-000371, Revision
 908 1. SAND2014-0187P. 89pp.

909 Van Loon, L.R., Glaus, M.A., Müller, W. 2007. Anion exclusion effects in compacted
 910 bentonites: Towards a better understanding of anion diffusion. In: Clays in natural &
 911 engineered barriers for radioactive waste confinement International meeting,
 912 september 2007, lille, france, andra ed, pp 123-124.

913 Watson, C., Hane, K., Savage, D., Benbow, S., Cuevas, J., Fernández, R. 2009. Reaction
 914 and diffusion of cementitious water in bentonite: Results of 'blind' modelling. Applied
 915 Clay Science, 45, 54–69.

916 Wersin, P., Birgersson, M., Olsson, S., Karnland, O., Snellman, M., Saanio & Riekkola Oy
 917 .2008. Impact of corrosion-derived iron on the bentonite buffer within the KBS-3H
 918 disposal concept. The Olkiluoto site as case study. SKB report R-08-34. 61 pp.

919 Wersin, P., Johnson, L.H. and McKinley I.G. 2007. Performance of the bentonite barrier
 920 at temperatures beyond 100°C: A critical review. Physics and Chemistry of the Earth
 921 32, 780-788.

922 Yang, C., Samper, J., Montenegro, L. 2008. A coupled non-isothermal reactive transport
 923 model for Long-term geochemical evolution of a HLW repository in Clay.
 924 Environmental Geology, 53, 1627-1638.

925 Yuan, Q., Shi, C., De Schutter, G., Audenaert, K., Deng, D. 2009. Chloride binding of
 926 cement-based materials subjected to external chloride environment – A review
 927 Construction and Building Materials 23, 1–13

928 Zhang, T., Cheeseman, C.R. and Vandeperre, L.J. 2011. Development of low pH cement
 929 systems forming magnesium silicate hydrate (M-S-H). Cement and Concrete Research,
 930 41, 439–442.

931 Zheng, L., Jové Colón, C., Bianchi, M., Birkhozler, J. 2014. Argillite/Shale Disposal
 932 Reference. Lawrence Berkeley National Laboratory. LBNL Paper LBNL-6709E.
 933 eScholarship. University of California. <http://escholarship.org/uc/item/11k6z4mh>. 49pp.

934

935 List of Figures

936 **Figure 1:** XRD patterns from oriented aggregates prepared with a
937 separated < 2µm size fraction of both bentonites, natural and pretreated.

938 **Figure 2:** Top: Picture showing the final configuration of the experiment
939 and a scheme of the cell. Bottom: Scheme of the six samples for the
940 experiments performed in small cells. FEBEX Natural in yellow, FEBEX
941 pretreated bentonite in blue and lime mortar in green.

942 **Figure 3:** Drawing of the different sampling schemes performed on small
943 cells. A, B: samples for water content and density. C: longitudinal cut for
944 preparing polished sections for microscopy inspection and analysis. D:
945 transversal sections to determine porosity, exchangeable cations and
946 soluble salts. U: longitudinal section to perform a detailed sampling for
947 mineralogy and external specific surface determinations. Comparison of a
948 dry polished section to a resin embedded polished section from lime mortar
949 bentonite interfaces experiments.

950 **Figure 4:** Mass balance of ions in the experiments. In the upper part:
951 hydration reservoir; Initial composition is subtracted from final. In the
952 lower part: the average final composition of the bulk material is
953 subtracted from the bentonite initial values; bp: bentonite pretreated; bn:
954 bentonite natural; fe: contains magnetite. All the values are calculated as a

function of the material mass inside the cells (mmol/100 g material). Note:

discontinuous bar for cell 1 in the water reservoir account for the lack of

data in this cell caused by a leakage during the dismantling operation.

Figure 5: Soluble ions and adsorbed iron. Upper part: chloride and sulfate distribution in cells 2 and 4 (bentonite natural and mortar- bentonite natural-magnetite). SEM-EDX images and analysis show evidences for precipitation of ettringite-like and gypsum minerals. Lower part: distribution of the total extracted iron along the columns in cells 1 to 6. Picture showing the appearance of cells 2 (no interfaces) and 4 (both interfaces) at the hydration zone once cells were dismantled.

Figure 6: Soluble and exchangeable cations distribution along the bentonite block in cells 2 and 4, both with natural FEBEX bentonite; and cell 3 with pretreated FEBEX bentonite (aqueous extract solid:liquid 1:8). Pretreated or natural in exchangeable cations figures are the initial values for the bentonite materials.

Figure 7: Total porosity and SSA BET distribution in cells 3 and 4 (upper part). In the lower part details for sampling and a sketch for the interpretation of the aggregation for bentonite particles and the sealing of micropores. Micro, micro and mesopores evolution are compared (natural bentonite without and with mortar) for data in cells 2 (sections 1, 2 and 3: D1, D2 and D3) and 4 (sections 1, 2, 3 and 4 are D1, D2, D3 and D4).

Figure 8: Back scattering mode SEM photographs taken from interfaces in cell material slices (L sections in Figure 11) embedded in LR-WHITE resin and polished; a) cell 3 (pretreated bentonite two interfaces); b) cell 4 (natural bentonite two interfaces); c)

cell 5(pretreated bentonite one mortar interface; d) cell 6 (pretreated bentonite one magnetite interface. In cell 6 just magnified details of granular magnetite-bentonite contact are shown.

Figure 9: Chemical profiles (Al, Ca, Mg and K) in the bentonite-mortar. The vertical line in the figures from the upper part marks the interface location.

Figure 10: X-ray powder patterns for randomly oriented powder bulk samples for selected samples in cells 1,2,3,4 and 5 (1, 3 and 5 pretreated FEBEX), and 2, 4: natural FEBEX bentonite. See Table VI. Sm: smectite, Clay: clay minerals, Qtz: quartz, Kfs: K-feldspars, Pl: Plagioclase, Cal: calcite. CH: portlandite, C-S-H: low crystalline calcium silicate hydrate Ca/Si ~1. Numbers above the reflections are d-spacings in Å.

List of Tables

Table I: Exchangeable cations and BET surface (SBET) for the natural and pretreated FEBEX bentonites. Characteristics of lime mortar prepared for the experiments.

Highlights:

Holistic experimental approach evidencing mass transfer processes occurring in the EBS of a DGR at the repository conditions prevailing from 1000 to 3000 years after emplacement.

The potential capacity of concrete and iron corrosion products interfaces to act as a sink of soluble salts were investigated

The positive role of exchangeable Mg buffering capacity regarding the neutralization of the alkaline plume in the EBS system was established.

A low porosity bentonite-cement mortar zone was experimentally created: consequences in decreasing the hydration rate of the bentonite and hence RN transport could be significant.

The availability for exchangeable K^+ uptake from cementitious materials, affecting initially the bentonite hydration and swelling was investigated.

Table I: Exchangeable cations and BET surface (SBET) for the natural and pretreated FEBEX bentonites. Characteristics of lime mortar prepared for the experiments

FEBEX	Na ⁺ (cmol(+)/Kg)	K ⁺ (cmol(+)/Kg)	Ca ²⁺ (cmol(+)/Kg)	Mg ²⁺ (cmol(+)/Kg)	Total (cmol(+)/Kg)	SSA BET (m ² /g)
Natural	26 ± 2	2.3 ±0 .1	36 ± 2	37 ± 3	102± 5	56 ± 0.5
Pretreated	6.5 ± 0.3	31 ±0.5	43 ± 2	1.8 ± 0.2	81± 2	58 ± 2
MORTAR	Porewater pH	Water content weight %	Dry density g/cm ³	Calculated porosity V %	Hg intrusion porosity(*) v%	Ca(OH) ₂ weight %
	12.6	22.9	1.55	35.4	33.3	39.8

*: As measured in a Micromeritics™ AutoPore IV 9500 V1.05 apparatus

Figure 1
[Click here to download Figure: Figure 1.pptx](#)

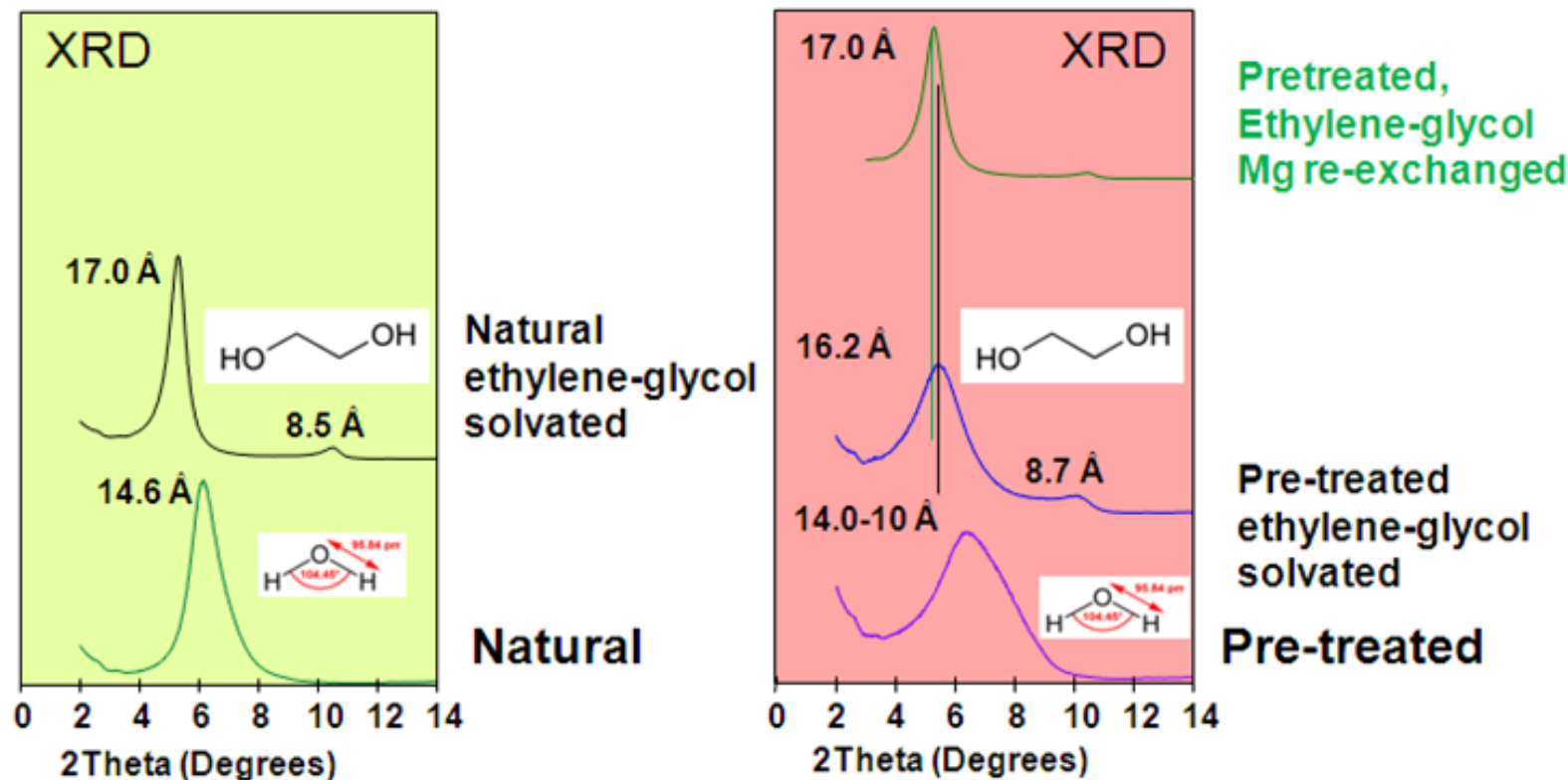


Figure2
[Click here to download Figure: Figure 2new.pptx](#)

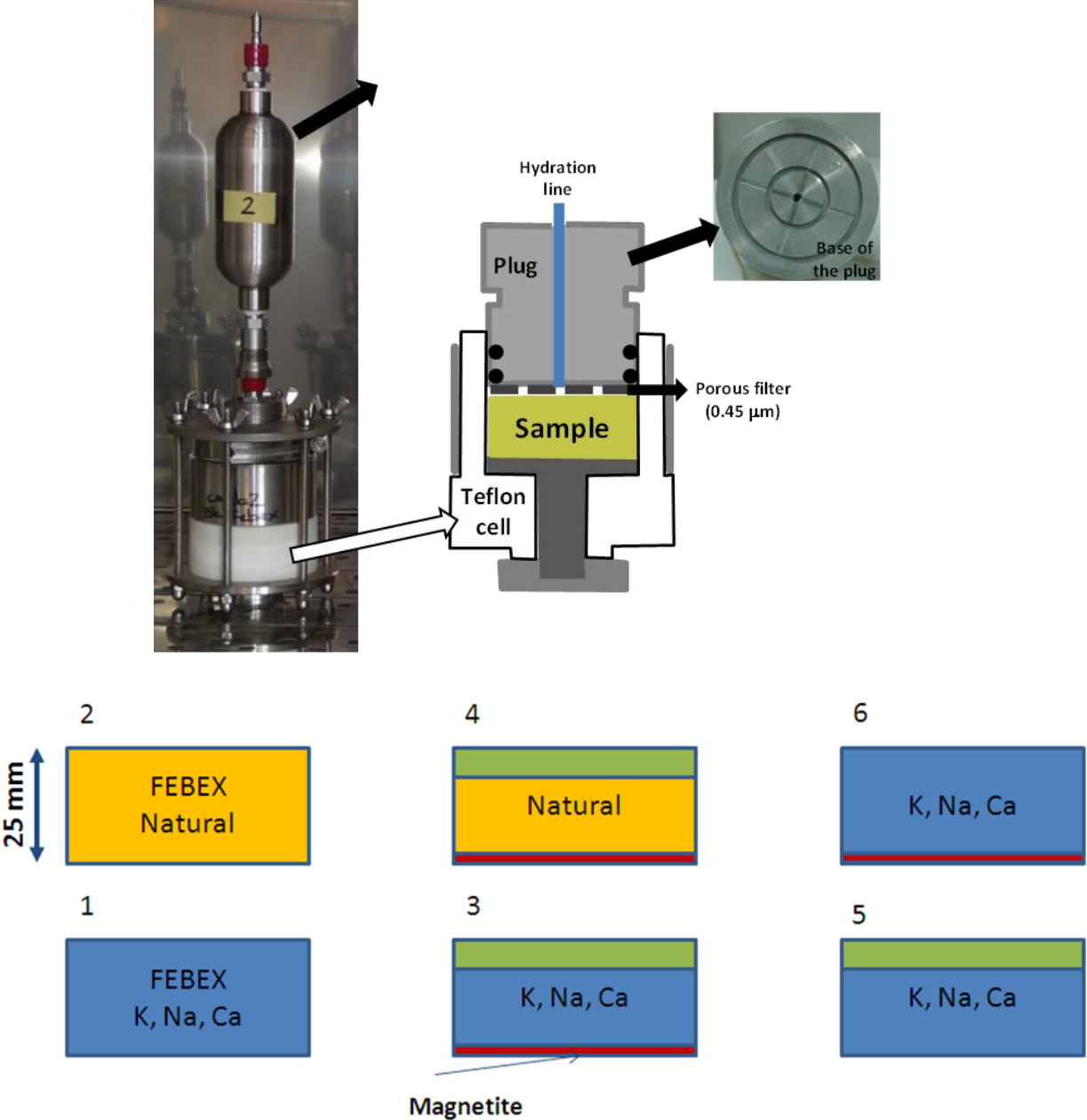
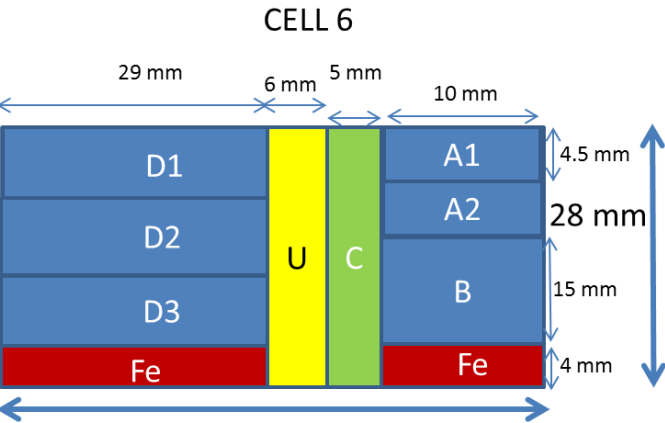
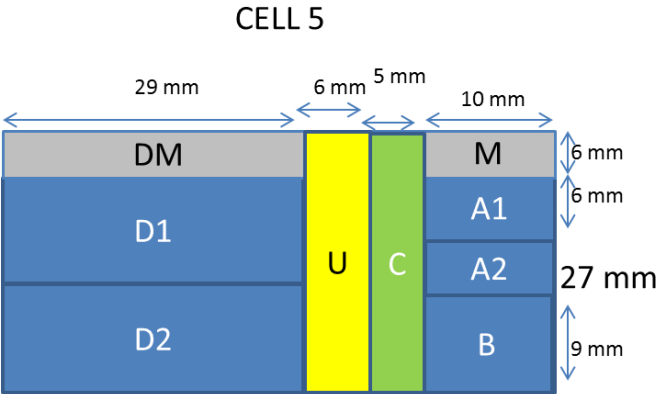
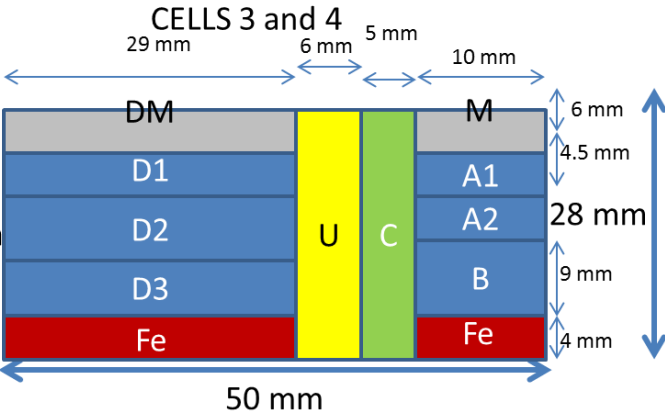
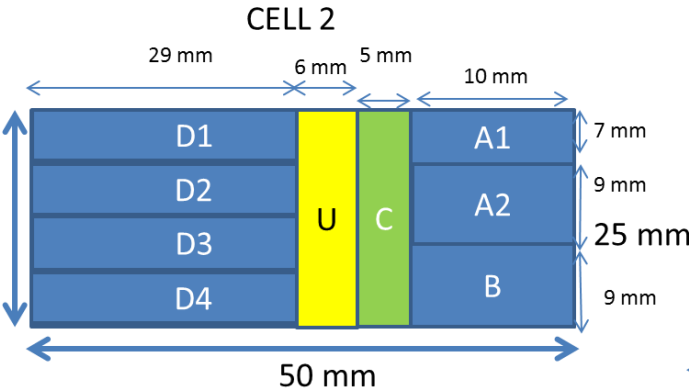
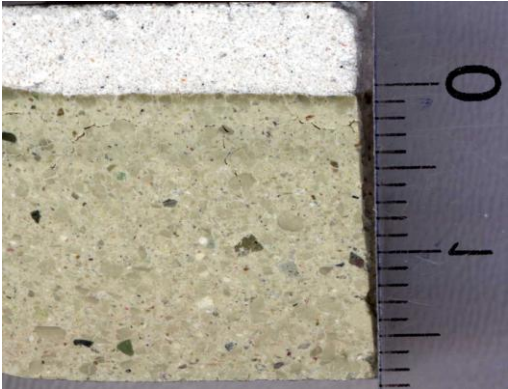


Figure3
[Click here to download Figure: Figure 3new.pptx](#)



C sections
Vacuum dried cell 3



Resin embedded cell 5

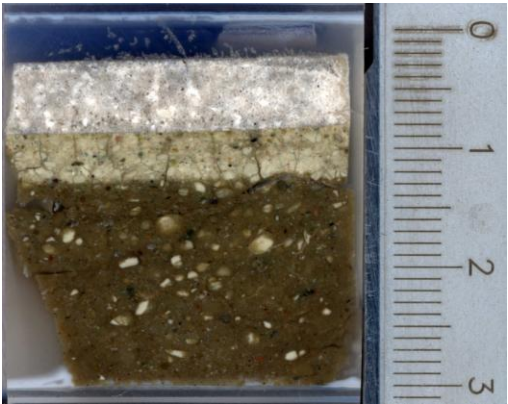


Figure 4
[Click here to download Figure: Figure 4.pptx](#)

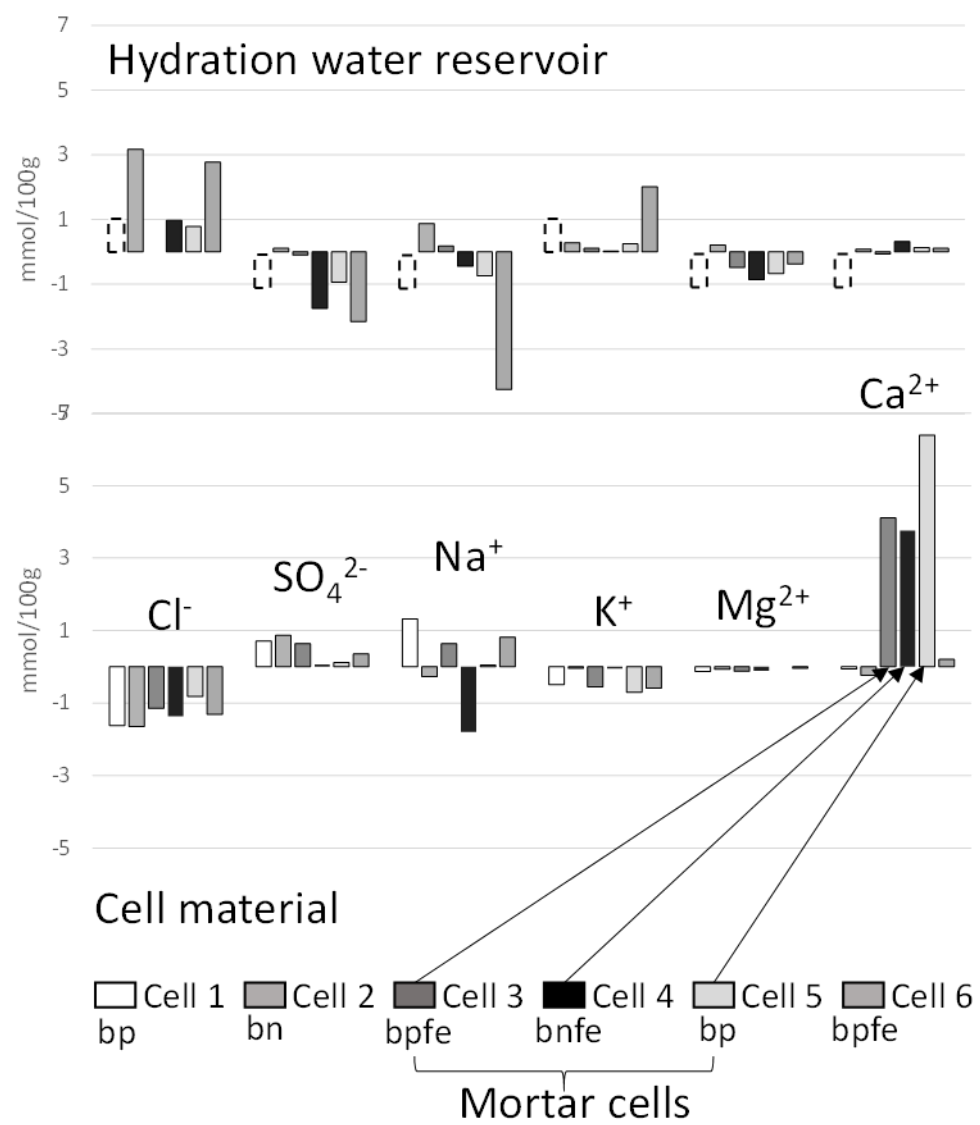


Figure 5
[Click here to download Figure 5.pptx](#)

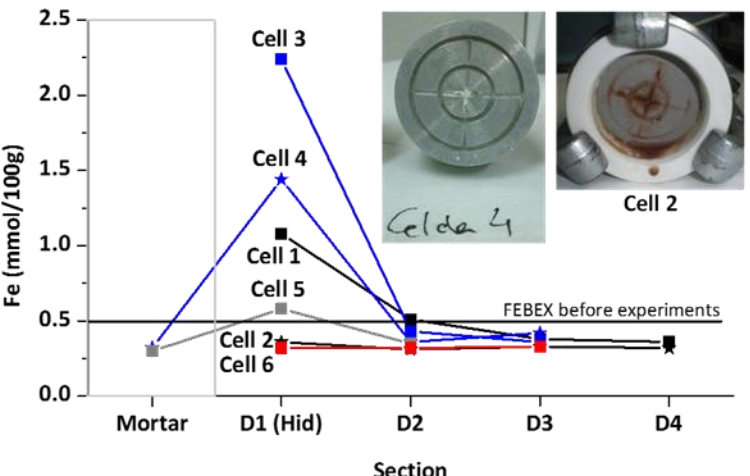
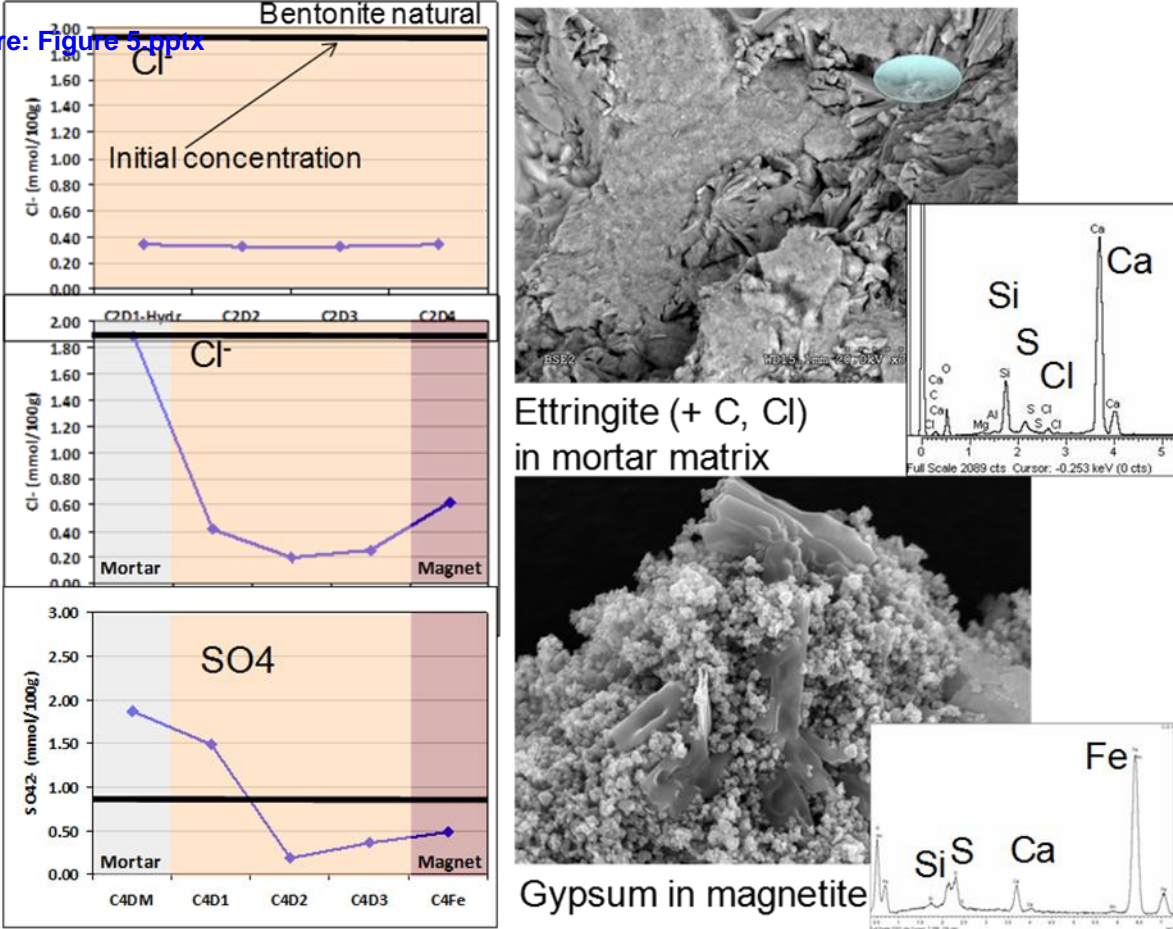
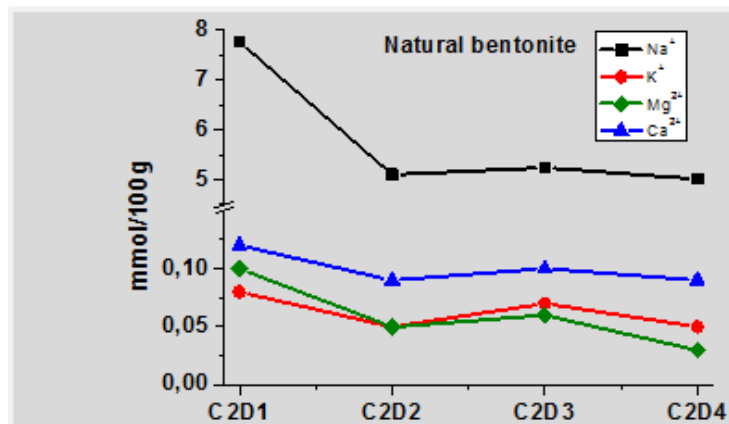


Figure 6

[Click here to download Figure 6.pptx](#)

SOLUBLE CATIONS



EXCHANGEABLE CATIONS

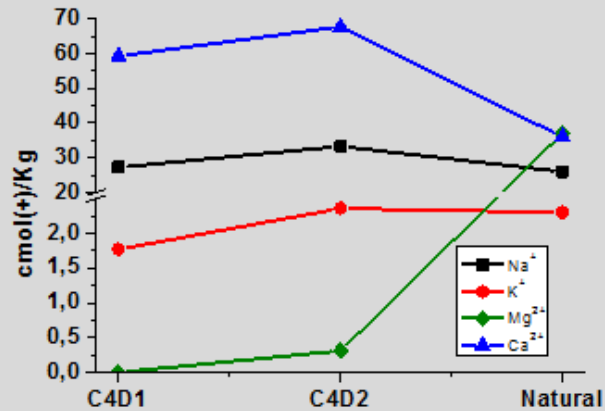
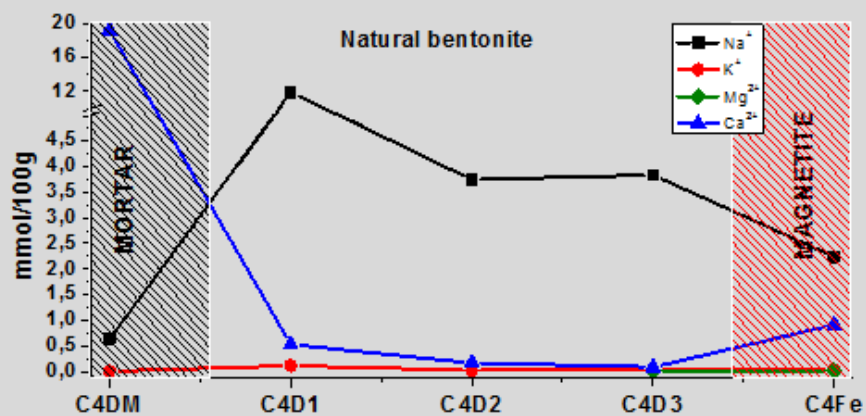
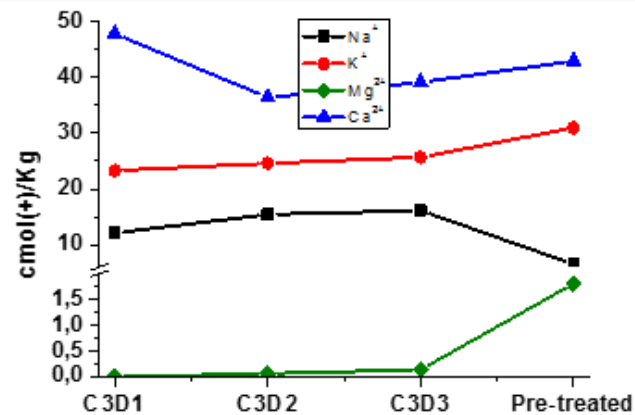
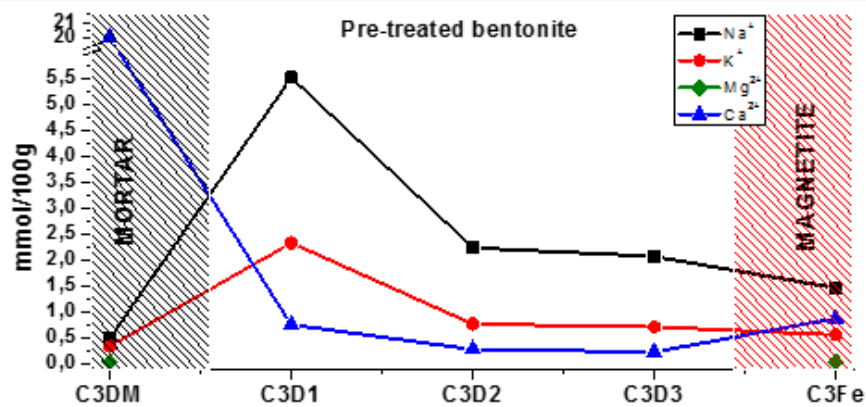
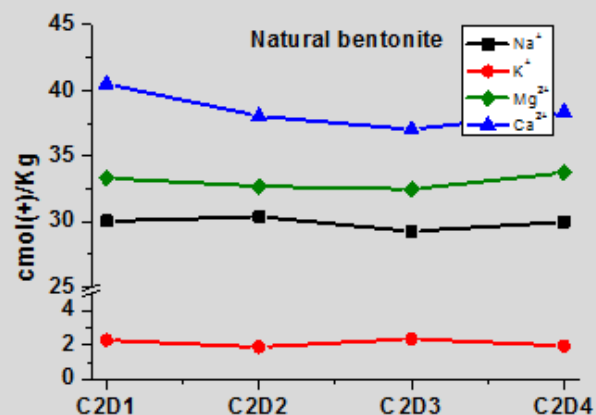


Figure 7

[Click here to download Figure: Figure 7.pptx](#)

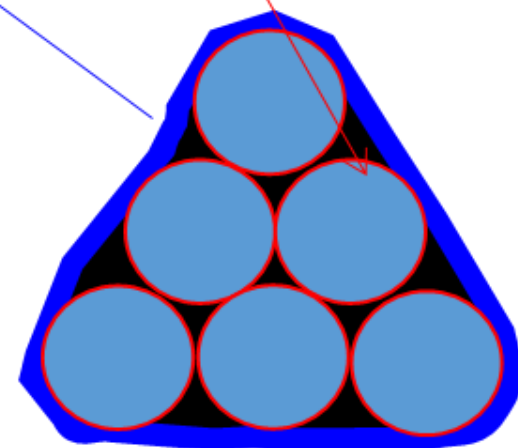
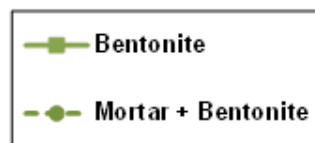
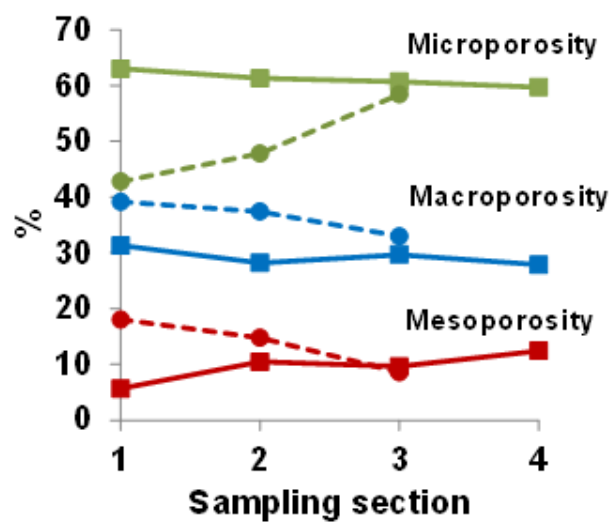
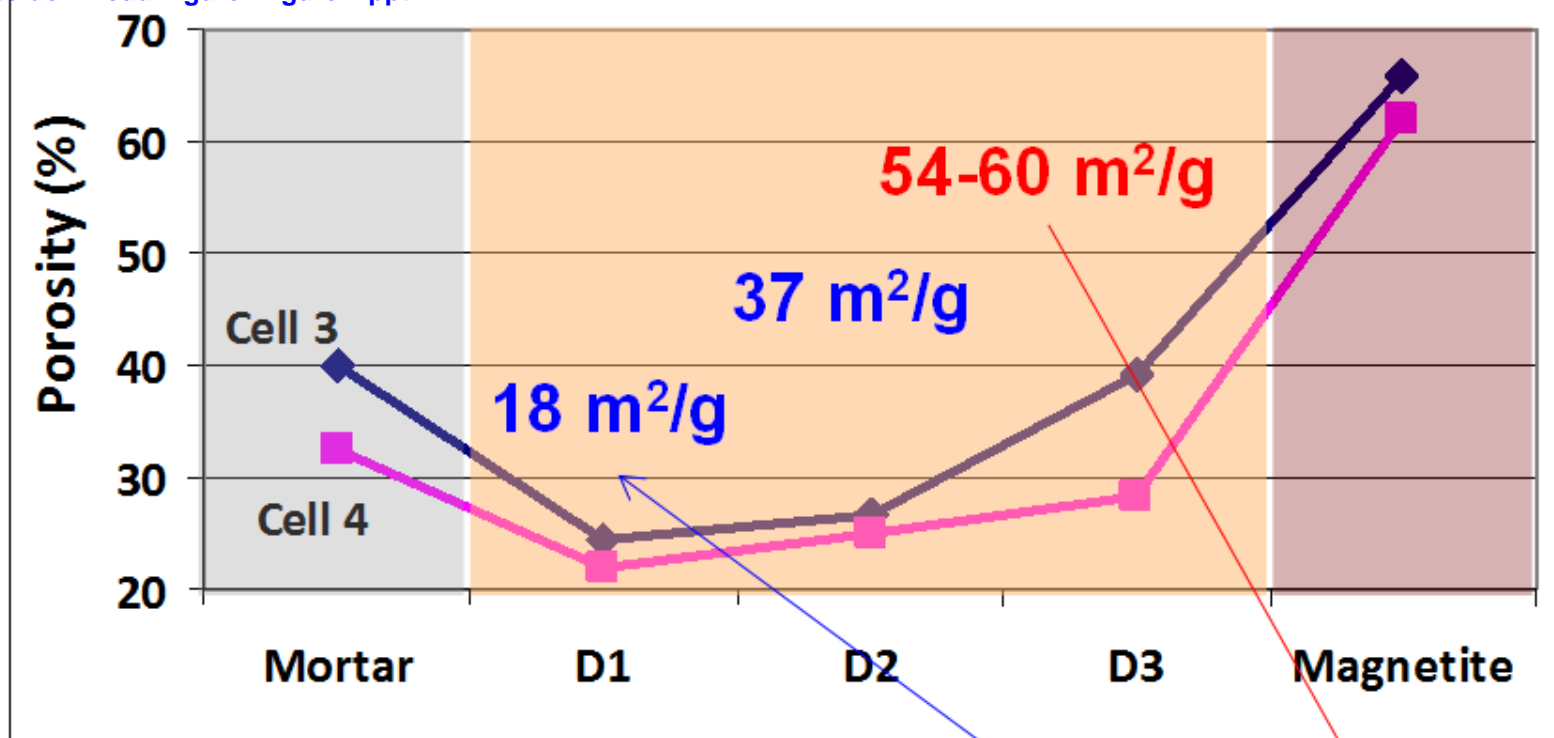


Figure 8
[Click here to download Figure: Figure 8.pptx](#)

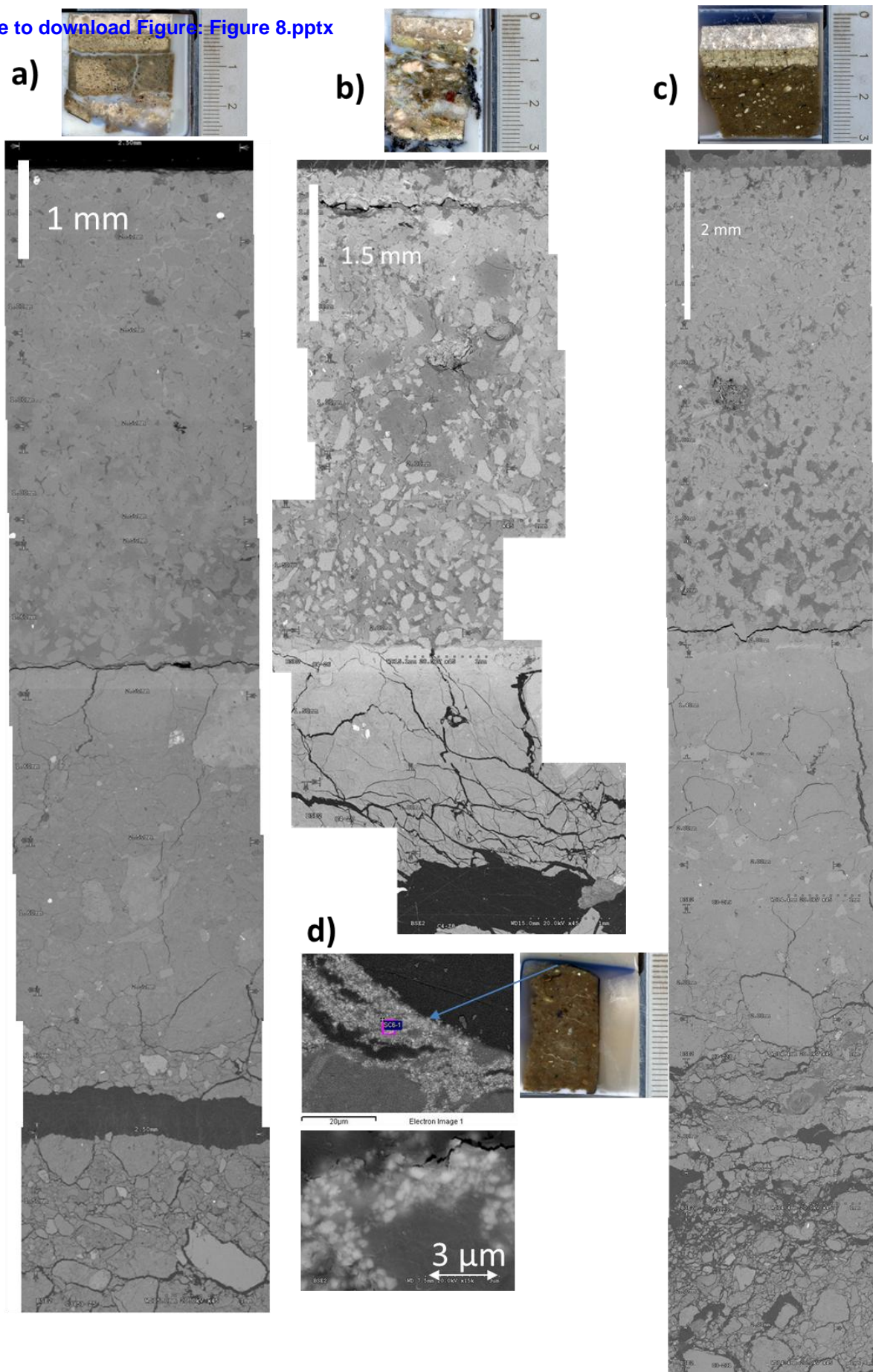


Figure 9

[Click here to download Figure: Figure 9.pptx](#)

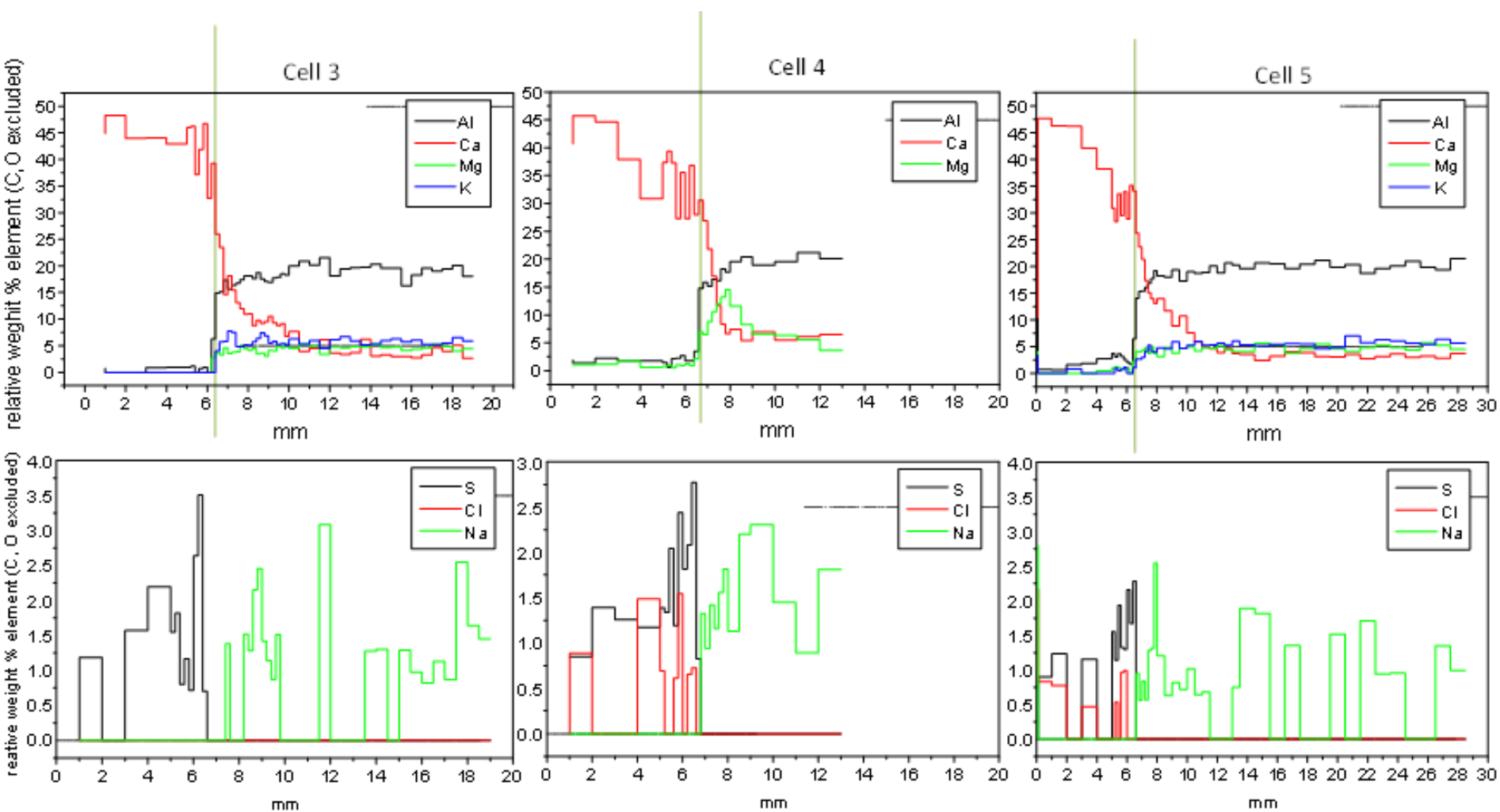
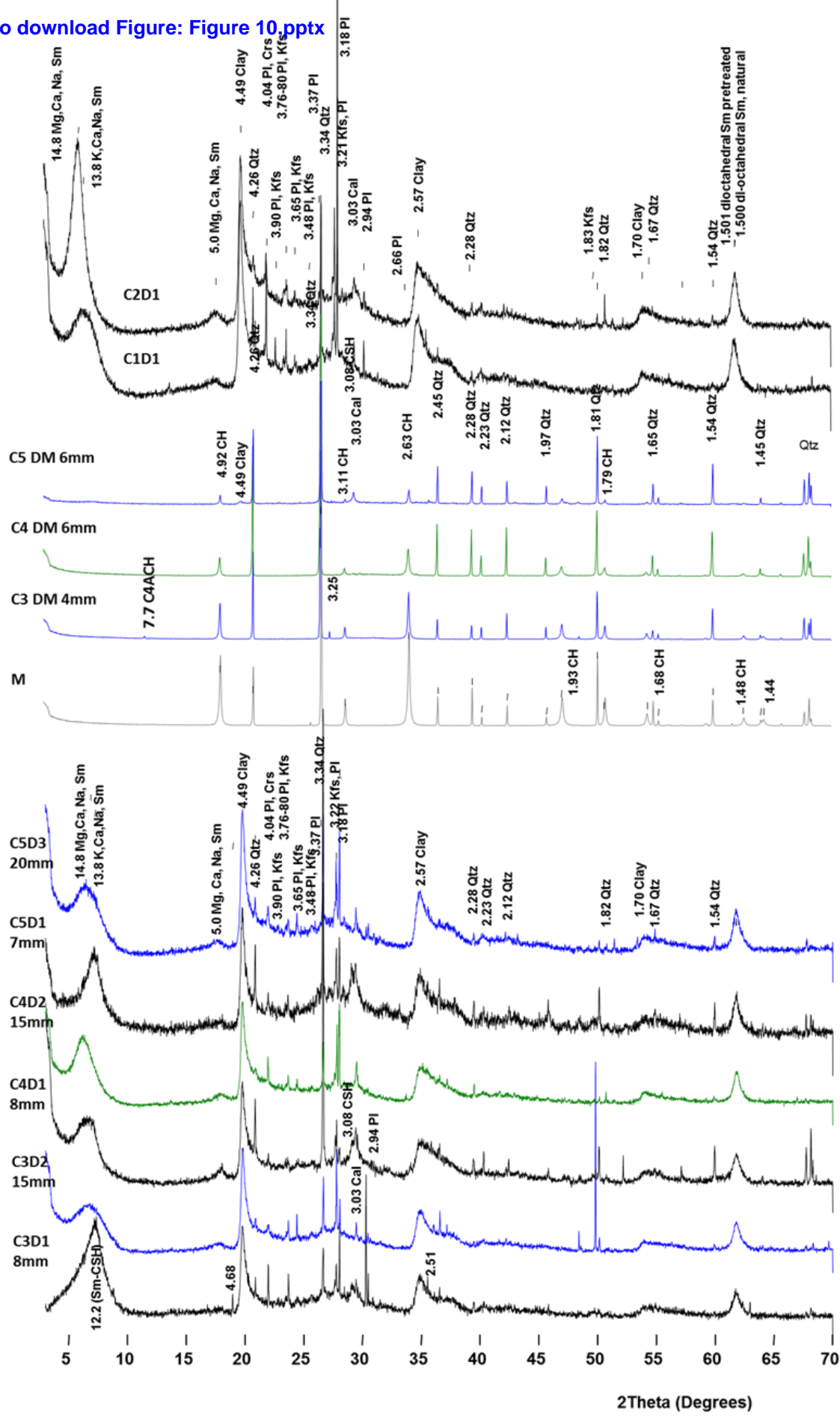


Figure 10
[Click here to download Figure: Figure 10.pptx](#)



1 **Abstract**

2 The aim of this study was to obtain evidences regarding the physical and geochemical
3 processes occurring as a result of the combined effects of cementitious materials from
4 the concrete degradation and magnetite from steel corrosion on the bentonite barrier
5 during disposal of high-level radioactive waste.

6 A series of six experiments were done that attempt to reproduce the repository
7 conditions prevailing from 1000 to 3000 years after emplacement of wastes. A lime
8 mortar was used as the source of calcium and alkalinity as this is the presumed
9 reactive product produced during concrete degradation at long-term. Magnetite
10 powder was used to simulate the final corrosion product of cast iron and C-steel under
11 anaerobic conditions. Either a natural FEBEX bentonite or a pretreated “aged” sample,
12 depleted in exchangeable Mg and enriched in K, were used as the swelling clay
13 component. Experiments, with both types of bentonite, were performed
14 simultaneously in cylindrical specimens (50 mm diameter, 25 mm length), confined in a
15 Teflon® sleeve/steel case cells. These specimens were composed of cement mortar in
16 contact with compacted bentonite, which was in turn in contact with compressed
17 magnetite powder. They were hydrated with an artificial $\text{Na}^+\text{-Ca}^{2+}\text{-SO}_4^{2-}$ -type Spanish
18 reference clayey formation water for 18 months at 60 °C and constant hydraulic
19 pressure applied through the base of the mortar..

20 After dismantling and sampling the specimens, distribution of soluble ions,
21 exchangeable cations and mineralogy were studied in the bentonite by different
22 instrumental techniques. Iron migration or any impact of the corrosion products in the
23 bentonite was not noticeable in the clay. Both, mortar and magnetite acted as sinks of

24 chloride and sulfate. Small quantities of Ca-Al-sulfates and carboaluminates, which can
25 allocate chlorides, were determined near the mortar-bentonite interface. Portlandite
26 dissolved near the bentonite interface and induced the formation of calcium silicates
27 hydrates (C-S-H) phases cementing the clay interface characterizing a calcium front
28 that was developed from the mortar towards the bentonite. Magnesium silicate
29 hydrates (M-S-H) phases were also concentrated at the interface with mortar in the
30 natural bentonite. It was also determined that natural bentonite has potentially higher
31 buffering capacity attenuating the calcium alkaline front than the pretreated clay. In
32 both cases, a low porosity bentonite-mortar zone was experimentally created at the
33 interface. This type of material should be carefully studied in order to predict the
34 potential for further development of a diffusive alkaline alteration, the radionuclides
35 retention and the consequences in the hydration rate of the unaffected bentonite
36 buffer.

Background dataset for online publication only

[Click here to download Background dataset for online publication only: Additional information_2016_corrected.docx](#)